© 2023. Published by The Company of Biologists Ltd | Journal of Cell Science (2023) 136, jcs260442. doi:10.1242/jcs.260442

RESEARCH ARTICLE

Matrix stiffness regulates Notch signaling activity in endothelial cells

Maibritt Kretschmer[1], Rose Mamistvalov[2], David Sprinzak[2], Angelika M. Vollmar[1] and Stefan Zahler[1,*]

ABSTRACT

Notch signaling is critical for many developmental and disease-related processes. It is widely accepted that Notch has a mechanotransduction module that regulates receptor cleavage. However, the role of biomechanical properties of the cellular environment in Notch signaling in general is still poorly understood. During angiogenesis, differentiation of endothelial cells into tip and stalk cells is regulated by Notch signaling, and remodeling of the extracellular matrix occurs. We investigated the influence of substrate stiffness on the Notch signaling pathway in endothelial cells. Using stiffness-tuned polydimethylsiloxane (PDMS) substrates, we show that activity of the Notch signaling pathway inversely correlates with a physiologically relevant range of substrate stiffness (i.e. increased Notch signaling activity on softer substrates). Trans-endocytosis of the Notch extracellular domain, but not the overall endocytosis, is regulated by substrate stiffness, and integrin cell–matrix connections are both stiffness dependent and influenced by Notch signaling. We conclude that mechanotransduction of Notch activation is modulated by substrate stiffness, highlighting the role of substrate rigidity as an important cue for signaling. This might have implications in pathological situations associated with stiffening of the extracellular matrix, such as tumor growth.

KEY WORDS: Substrate stiffness, Mechanosensing, Endothelial cells, Notch1, Dll4

INTRODUCTION

The Notch signaling pathway plays a crucial role in many tissues, regulating cell fate decisions, cell cycle progression and apoptosis during tissue development and maintenance (Liu et al., 2003; Totaro et al., 2018). Notch signaling is induced by a Notch ligand (Delta-like 1, Delta-like 4 or Jagged 1) interacting with one of four types of Notch receptors (Notch1–4) of an adjacent cell (trans interaction), which triggers a signaling cascade in the receiver cell (Boareto et al., 2015; Sprinzak et al., 2010; Totaro et al., 2018). Receptor–ligand binding leads to two receptor proteolytic cleavage events, resulting first in separation of the Notch extracellular domain (NECD) and subsequently in release of the Notch intracellular domain (NICD) (Hodkinson et al., 2007; Nandagopal et al., 2018; Nichols et al., 2007). The NECD is pulled into the ligand-presenting cell (sender cell) along with the ligand in the course of trans-endocytosis, while the NICD is translocated to the nucleus of the receiver cell, where it associates with the transcriptional regulator RBPJ, activating the Notch target genes such as those encoding hairy and enhancer of split (HES) transcription factors and HES-related proteins (Hodkinson et al., 2007; Liu et al., 2003; Meloty-Kapella et al., 2012).

During Notch signaling activation, mechanical forces generated by endocytosis in the sender cell are required for opening the negative regulatory region (NRR) in the Notch receptor, which leads to the first proteolytic cleavage event (Koon et al., 2018; Meloty-Kapella et al., 2012). However, the influence of mechanical cues from the surrounding matrix on this process (i.e. mechanosensitivity) is poorly studied.

The Notch signaling pathway is instrumental for angiogenesis, regulating the selection of tip and stalk cells (Antfolk et al., 2017; Merk et al., 2016). Of the four Notch receptor homologs and five Notch ligands that have been identified in mammals, the Notch receptor Notch1 and the ligands Dll4 and Jag1 are mainly involved in specification of tip and stalk cells (Antfolk et al., 2017; Stepanova et al., 2021; Totaro et al., 2018). Tip cells are characterized by increased Dll4 expression mediated by VEGFA–VEGFR2 (KDR) signaling (Antfolk et al., 2017; Stepanova et al., 2021). Stalk cells, on the other hand, exhibit increased Notch1 expression, and this is associated with the high Dll4 level in the tip cells. Activation of the Notch signaling pathway in stalk cells by Dll4 expression in tip cells induces cell proliferation of stalk cells, resulting in extension of sprouts and lumen formation (Pauty et al., 2018; Stepanova et al., 2021). Dll4–Notch1 signaling is antagonized by the ligand Jag1, which prevents the activation of Notch receptors in stalk cells and promotes tip cell selection and sprouting by Jag1–Notch signaling (Andrawes et al., 2013; Antfolk et al., 2017). Whereas the biochemical cues during angiogenesis are well studied, the mechanical forces during angiogenesis are only beginning to be understood (Mammoto et al., 2009; Santos-Oliveira et al., 2015). Other than the shear force due to blood flow, most of the mechanical cues during angiogenesis are exerted by the extracellular matrix (ECM) and are caused by matrix structural changes that can locally alter the ECM stiffness and density (Fischer et al., 2009; Perfahl et al., 2017; Shamloo et al., 2016). However, little is known about the mechanical influences via the matrix on the signaling pathways involved in angiogenesis, such as the Notch signaling pathway.

In this study, we investigate the influence of different physiologically relevant substrate stiffnesses on the Notch signaling pathway and related pathways in endothelial cells, such as Yes-associated protein (YAP, also known as YAP1) signaling and adhesion-dependent signaling. Using different stiffness-tuned silicone substrates and two different modes of Notch activation with Dll4 as a ligand (via cell–cell contact or a protein coat), we show that activation of the Notch signaling pathway is stiffness dependent.

[1]Department of Pharmacy, Pharmaceutical Biology, Ludwig-Maximilians-Universität München, Butenandtstraße 5-13, 81377 Munich, Germany. [2]The George S. Wise Faculty of Life Sciences, Tel Aviv University, Tel Aviv 69978, Israel.

*Author for correspondence (stefan.zahler@cup.uni-muenchen.de)

D.S., 0000-0001-6776-6957; S.Z., 0000-0002-5140-7287

Handling Editor: Andrew Ewald
Received 18 July 2022; Accepted 22 December 2022

Journal of Cell Science (2023) 136, jcs260442. doi:10.1242/jcs.260442

Furthermore, we investigate the influence of cell–cell contacts on Notch activation and the mutual influence of Notch and cell–cell or cell–matrix adhesion proteins, as well as the crosstalk between Notch and YAP signaling, a well-known mechanosensitive pathway (Totaro et al., 2018). Taken together, our results demonstrate a mechanosensitivity of the Notch signaling pathway that is likely associated with the process of trans-endocytosis upon Notch activation by juxtacrine signaling, suggesting a second mechanical aspect of the Notch signaling pathway in addition to the pulling force generated by the ligand-presenting cell.

RESULTS

Decreased substrate stiffness increases Notch signaling activity in endothelial cells

To investigate the mechanosensitivity of the Notch signaling pathway, synthetic polydimethylsiloxane (PDMS) substrates with defined stiffness in a range from 0.5 to 70 kPa were applied. Endothelial cells [human umbilical vein endothelial cells (HUVECs) and mouse cardiac endothelial cells (MCECs)] were used as prototypic models for Notch signaling. The Notch signaling pathway was not additionally induced or was activated either via seeding of HUVECs onto a coat of recombinant humanDll4 (rhDll4) or by co-culture of HUVEC cells (receiver cells) with Dll4-overexpressing MCECs (MCEC-Dll4–mCherry; sender cells). Due to the dependence of the primary endothelial cells in *in vitro* culture on a protein coat, all substrates were coated with collagen type I, unless stated otherwise. The purified native collagen type I solution formed a 3D matrix on the substrates and thus enabled uniform adhesion of the endothelial cells. Analysis of a Notch dual luciferase reporter gene assay, which allowed for compensation of potentially varying transfection efficiencies in the primary HUVECs, showed a continuous increase in Notch transcriptional activity on softer substrates both without additional induction of the pathway and after activation either by cell–cell contact using the Dll4-overexpressing cell line or by an rhDll4 protein coating (Fig. 1A–C). However, the differences in Notch transcriptional activity on the various substrates without Notch induction were only minor, especially in contrast to the results after Notch activation. These findings were supported by intensity analysis of the nuclear localization of the NICD after immunofluorescence staining: the softer the substrate, the higher the NICD intensity in the Notch receiver cells upon stimulation (Fig. 1D–F). However, it must be kept in mind that the analysis of stained cells is limited by cell numbers (≥240 in our case) and is not a bulk measurement. Furthermore, results from RT-qPCR experiments showed that mRNA expression of the Notch target gene *Hey1* in HUVEC cells was increased on very soft substrates after Notch activation by an rhDll4 coat (Fig. S1C). mRNA expression of the ligand Dll4 showed a stiffness-dependent effect, whereas mRNA expression of the ligand Jag1 remained unchanged in the endothelial cells throughout the examined range of substrate stiffness (Fig. S1C). Thus, Notch activation, both by plate-bound Dll4 and by co-cultured sender cells, exhibits mechanosensitivity. Experiments measuring activation of the Notch signaling pathway upon co-culture with MCEC-Dll4–mCherry cells in different ratios, using either HUVEC cells or wild-type MCECs (MCEC-WTs) as signal receiver cells, showed a sender:receiver cell ratio of 1:1 to be optimal for activation. With a higher amount of sender cells, the overall signal intensity decreased (Fig. S2A,B). Human microvascular endothelial cells (HMECs) were used as an additional endothelial cell model; after co-culture with MCEC-Dll4–mCherry cells they showed results comparable to those obtained using HUVECs and MCECs, including the same mechanosensitivity (Fig. S2C).

To test for general effects of the different substrates on cell viability or proliferative capacity, the proliferation of HUVEC cells on substrates of different stiffness was investigated over periods of 24 h and 48 h. No differences in proliferation rates were detected (Fig. S1A). The efficiency and reproducibility of coating of the PDMS substrates with rhDll4 were controlled in an availability assay by immunostaining, which showed that the rhDll4 coat was evenly distributed and displayed a comparable intensity on all substrates (Fig. S1B).

Active integrin β1 increases on softer substrates and is influenced by Notch

Since interaction with the ECM is known to be mediated by integrin signaling, we next checked whether Notch signaling affects or is affected by integrins (Hodkinson et al., 2007). Integrin β1 (also known as ITGB1) represents the largest subchain of integrins and is involved in several biological processes, such as adhesion, migration and cell cycle regulation (Lei et al., 2008). Due to the involvement of β1 subchains in cell–ECM interaction, integrin β1 plays a major role, especially in endothelial cells (Howe and Addison, 2012). To investigate whether mechanosensitivity of Notch lies upstream or downstream of integrin signaling, we quantified total and activated β1 integrin levels with and without pretreatment of cells with the Notch inhibitors DAPT and SAHM1 on the different substrates. No cytotoxic effect of the inhibitors on HUVEC cells was detectable at the concentrations used (Fig. S1D,E). Previous studies have shown that levels of activated integrins, but not overall integrin levels, are substrate dependent and are increased on softer substrates (Du et al., 2011). Accordingly, in our model the overall intensity of integrin β1 in HUVEC cells did not change on the different substrates and was not affected by inhibition of the Notch signaling pathway with DAPT or SAHM1 (Fig. 2A,B). In contrast, the softer the substrate, the more integrin β1 was activated (Fig. 2C,D). Upon blocking of basal Notch1 cleavage by DAPT treatment, and thus downstream of Notch signaling, integrin β1 activation decreased substantially, although the correlation between softer substrates and increased integrin β1 activation remained to a small degree. A comparable effect was observed after Notch complex assembly was prevented by treatment with the alternative Notch inhibitor SAHM1 (Fig. 2C). Thus, Notch signaling occurs upstream of integrin activation, as far as mechanosignaling is concerned. This result was confirmed in the second endothelial cell line, MCEC-WT (Fig. S3A).

YAP signaling and Notch are inversely mechanoregulated

The role of YAP as a mechanotransducer, and the related mechanosensitivity of the YAP–TAZ (WWTR1) signaling pathway are well known (Matsuo et al., 2021; Nukuda et al., 2015). We and others have shown that YAP activity decreases on soft substrates (Gegenfurtner et al., 2018). To assess a possible YAP–Notch crosstalk in endothelial cells, we performed immunofluorescence staining in HUVEC cells seeded on plastic and PDMS substrates, again with and without addition of DAPT (25 µM, 24 h) or SAHM1 (10 µM, 24 h). As expected, our results show progressively decreased nuclear YAP intensity in HUVEC cells on softer substrates, demonstrating the mechanosensitivity of the YAP–TAZ signaling pathway in our cells (Fig. 3A,C). However, inhibition of the Notch signaling pathway had no clear effect on nuclear YAP intensity; only on the softest substrate of

Journal of Cell Science (2023) 136, jcs260442. doi:10.1242/jcs.260442

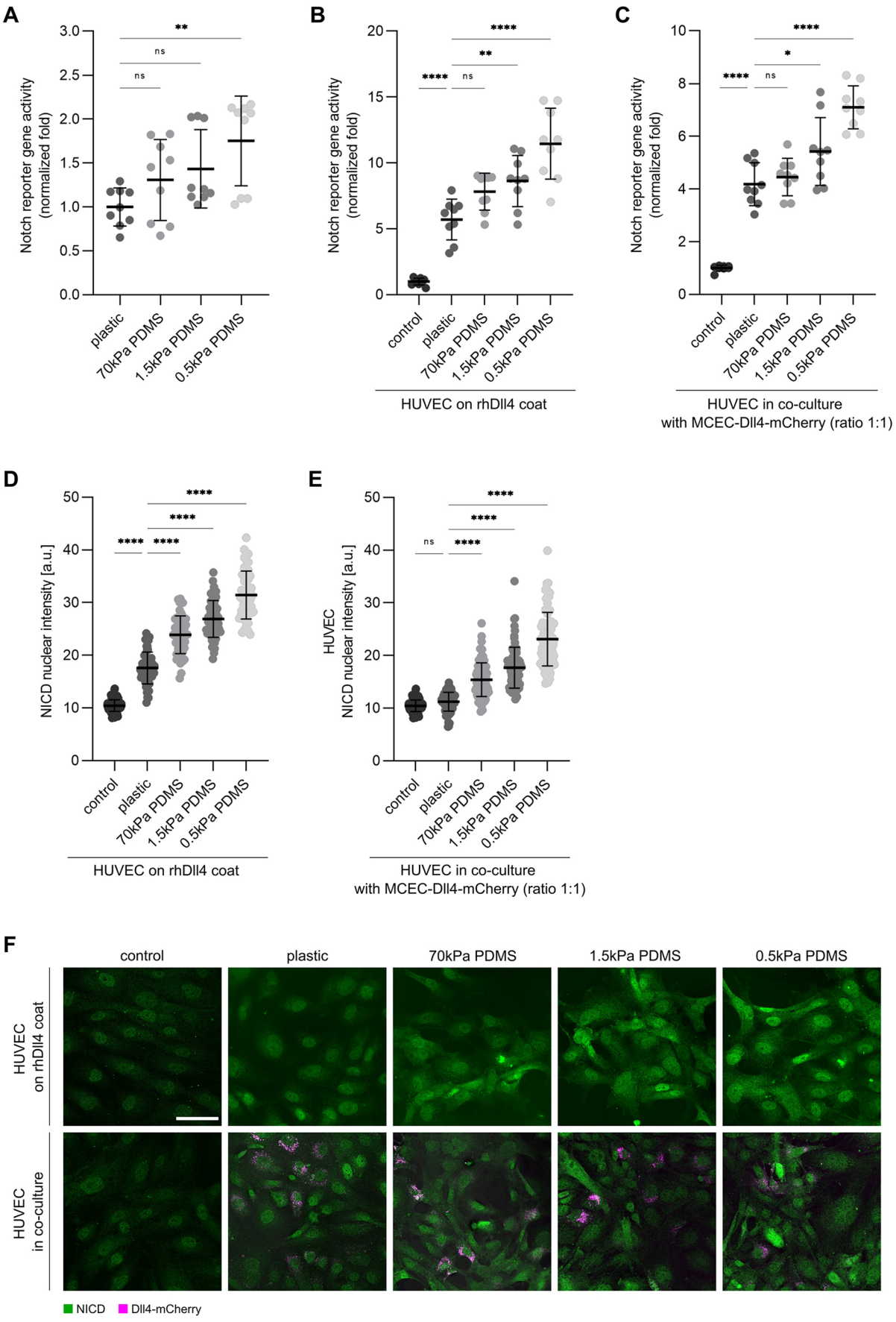

Fig. 1. See next page for legend.

Journal of Cell Science

Journal of Cell Science (2023) 136, jcs260442. doi:10.1242/jcs.260442

Fig. 1. Notch activity in endothelial cells increases on softer substrates. (A–C) Normalized fold change in Notch activity in confluent HUVEC cells on plastic or PDMS substrates with different stiffnesses, as indicated. Notch activity was determined by detection of cellular luciferase levels under control of the TP1-Luc Notch reporter. Data from three independent experiments, each with triplicates, are shown in scatter plots as mean±s.d. *P<0.1; **P<0.01; ****P<0.0001; ns, not significant (one-way ANOVA followed by Tukey's multiple comparison test). (A) No additional induction of Notch activity. (B) Induction of Notch activity by coating with rhDll4. Data were normalized to cells on plastic without Notch induction (control). (C) Induction of Notch activity by co-culture with MCEC-Dll4–mCherry cells on a collagen G coat. Data were normalized to cells on plastic without Notch induction (co-culture with untransfected HUVEC cells). (D,E) Nuclear NICD intensities (a.u., arbitrary units) in HUVEC cells seeded onto different plastic and PDMS substrates, as indicated. Quantitative evaluation of nuclear fluorescence intensity of NICD was performed by analysis with the Intensity Ratio Nuclei Cytoplasm Tool plugin for ImageJ. (D) Induction of Notch activity by coating with rhDll4. Mean±s.d. of ≥240 cells derived from three independent experiments. ****P<0.0001 (one-way ANOVA followed by Tukey's multiple comparison test). Data were normalized to cells on plastic without Notch induction (control). (E) Induction of Notch activity by co-culture with MCEC-Dll4–mCherry cells on a collagen G coat. Intensities in HUVEC cells were quantified in ≥80 single cells derived from three independent experiments using ROIs transferred from the Hoechst counter staining. Mean±s.d. ****P<0.0001; ns, not significant (one-way ANOVA followed by Tukey's multiple comparison test). Data were normalized to cells on plastic without Notch induction (control). (F) Representative images of HUVEC cells stained for NICD (shown in green; mCherry–Dll4 reporter of MCEC-Dll4–mCherry cells is shown in magenta), as described in D,E. Scale bar: 50 µm.

0.5 kPa did Notch inhibition rescue YAP activation to some degree (Fig. 3B,C). Consistent results were obtained with the control cell line MCEC-WT (Fig. S3B). Since YAP and Notch activity are inversely regulated by substrate stiffness, there seems to be no direct crosstalk between these two signaling pathways in this context.

VE-cadherin levels and trafficking to cell–cell borders are not affected by substrate stiffness, although the morphology of cell–cell contacts changes

Since the Notch signaling pathway is contact dependent, we examined the influence of substrate stiffness on the major endothelial adhesion molecule VE-cadherin (also known as CDH5). No correlation between VE-cadherin intensity (i.e. overall VE-cadherin expression) and substrate stiffness was detected. The junction patterns, however, showed stiffness-related changes. The softer the substrate, the less often typically branched and interlinked junction patterns were observed at the cell–cell contacts, and a continuous VE-cadherin junction with a larger intensity area without branches or comb-like structures was visible instead, as shown in the representative images (Fig. 4A,B). We investigated the influence of substrate stiffness on VE-cadherin trafficking at cell–cell contacts using a fluorescence recovery after photobleaching (FRAP) assay. HUVEC cells were transiently transfected with a Citrine-coupled VE-cadherin plasmid and seeded on PDMS substrates with different stiffnesses. VE-cadherin recovered to the same extent and with the same kinetics on all substrates, and therefore, no significant differences in the half time of recovery were observed (Fig. 4C). Thus, the altered junction pattern on the different substrates does not depend on or affect VE-cadherin kinetics.

To investigate the importance of existing cell–cell contacts for basal Notch activity, we first acutely destabilized cell–cell contacts using EGTA and then inhibited them in a prolonged manner using a VE-cadherin-blocking antibody. Treated cells were stained for NICD, and its intensity was analyzed in the nuclei as readout for Notch activity. Because EGTA might affect the structural activity of Notch1, leading to receptor cleavage and activation (Rand et al., 2000; Tremblay et al., 2013), we checked the effect of EGTA on NICD levels in comparison to further blocking of VE-cadherin by an antibody. Basic activity of Notch was weak, and EGTA alone only marginally decreased NICD levels in the nucleus independently of stiffness. The VE-cadherin-blocking antibody enhanced this effect (Fig. 5A) independently of substrate stiffness. The representative images shown in Fig. 5A (0.5 kPa PDMS substrate) confirm the quantitative analyses and show that the treatment changed the cell morphology and caused the cells to drift apart, leading to diminished cell–cell contacts. This is, however, not surprising, since in this setting without further stimulation inherent Notch signaling completely depends on the physical contact between endothelial cells.

To also test for a possible effect of Notch on VE-cadherin, we treated cells with DAPT (25 µM, 24 h) or SAHM1 (10 µM, 24 h). The results show that there was a significant reduction in VE-cadherin intensity after Notch inhibition on all substrates, and the reduction was greater after treatment with SAHM1 compared to the effects of treatment with DAPT (Fig. 5B,D). The junction patterns, however, did not change following the addition of DAPT or SAHM1 (Fig. 5C,D). Thus, changes in VE-cadherin morphology due to substrate stiffness seem to be independent of Notch signaling, whereas overall VE-cadherin expression is not.

Decreased substrate stiffness elevates NECD trans-endocytosis but not general endocytosis

To investigate the role of Notch receptor–ligand binding in increased Notch signaling activity on softer substrates, we performed a trans-endocytosis assay (Shaya et al., 2017). Separate cell populations were transfected with either a Notch1–Citrine fusion plasmid or a doxycycline-controlled Dll4–mCherry fusion plasmid. Dll4 expression was induced by adding doxycycline to the co-culture of both transfected cell populations. Analysis was performed using ImageJ in the areas where the signals of Notch1 receptor and Dll4 ligand overlapped at the cell–cell contacts of a signal-sending and a signal-receiving cell. To quantify trans-endocytosis and examine the stiffness effects, the colocalization of Notch receptor and ligand was analyzed both in the form of intensity analysis of the overlay areas and as a correlation analysis using Pearson's r coefficient. Only the signal overlays of Notch1 extracellular domain and Dll4 that clearly occurred in the signal-sending cell were examined. Trans-endocytosis peaked after 6 h of incubation, as described previously by Shaya et al. (2017). Our results show that trans-endocytosis increased on soft substrates, which was reflected in an increased intensity of the interaction area as well as in a higher colocalization coefficient – the Pearson's r value (Fig. 6A). A transferrin endocytosis assay was performed on the substrates to exclude a stiffness effect on endocytosis in general. The results show that the softer substrates did not enhance general endocytosis, so the increased trans-endocytosis cannot be attributed to general increase in endocytosis (Fig. S4A). Thus, trans-endocytosis seems to selectively exhibit mechanosensitivity in cell–cell contact-dependent receptor binding. The same experiments were performed with the endothelial cell line MCEC-WT for comparison, showing similar results and the same effect: the softer the substrate, the more trans-endocytosis occurred upon cell–cell contact (Fig. S4B). Furthermore, trans-endocytosis was analyzed using a flow cytometry assay wherein the presence of double-positive cells (i.e. cells showing a signal in both the FITC

Journal of Cell Science (2023) 136, jcs260442. doi:10.1242/jcs.260442

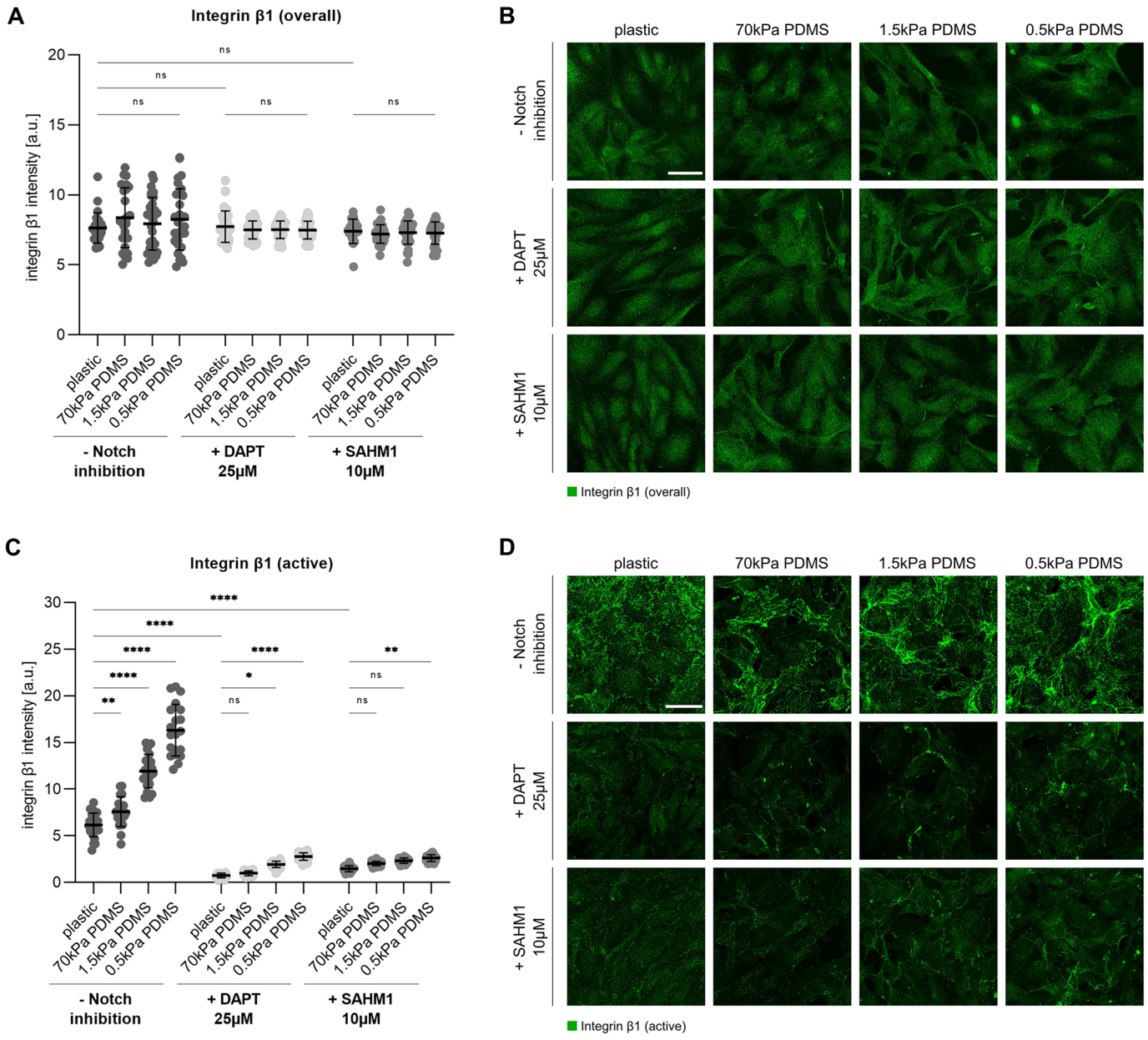

Fig. 2. Integrin β1 activity relates to substrate stiffness and is influenced by Notch. (A) Integrin β1 intensities in HUVECs. Cells were seeded on varying substrate stiffness, treated with 25 µM DAPT or 10 µM SAHM1 for 24 h, as indicated, and stained for total integrin β1. Mean±s.d. intensity of ≥240 cells derived from three independent experiments are depicted and compared to the integrin β1 intensities without Notch inhibition (a.u., arbitrary units). ns, not significant (one-way ANOVA followed by Tukey's multiple comparison test). Intensities were analyzed in segmented images. (B) Representative images of HUVEC cells on plastic and PDMS substrates with or without DAPT or SAHM1 treatment. Cells are stained for total integrin β1 (green). Scale bar: 50 µm. (C) Integrin β1 (active) intensity in HUVECs. Cells were seeded on varying substrate stiffness, treated with 25 µM DAPT or 10 µM SAHM1 for 24 h, as indicated, and stained for the activated form of integrin β1. Mean±s.d. intensity of ≥240 cells derived from three independent experiments are depicted and compared with the integrin β1 intensities without Notch inhibition. **P*<0.1; ***P*<0.01; *****P*<0.0001; ns, not significant (two-way ANOVA followed by Tukey's multiple comparison test). Intensities were analyzed in segmented images. (D) Representative images of HUVEC cells on plastic and PDMS substrates with or without DAPT or SAHM1 treatment. Cells are stained for activated integrin β1 (green). Scale bar: 50 µm.

and PI channels) indicates that trans-endocytosis has occurred. The results are in line with those obtained by confocal microscopy, with increased trans-endocytosis observed among cells cultured on softer substrates (Fig. 6B).

Nevertheless, Notch recipient cells also showed increased Notch signaling activity after activation by an rhDll4 coat, where no trans-endocytosis takes place. In order to investigate whether the stiffness effect of the Notch signaling pathway was also detectable in the absence of cell–cell contacts – and thus independently of trans-endocytosis and solely by Notch activation with rhDll4 – a dual luciferase reporter gene assay was performed in nonconfluent HUVECs, in contrast to the confluent cells used in the experiment shown in Fig. 1A. Again, the data were normalized to a transfection control to overcome the effects of both transfection and low cell density on the results. We observed a significant increase in reporter gene activity after Notch activation by rhDll4 on softer substrates

Journal of Cell Science (2023) 136, jcs260442. doi:10.1242/jcs.260442

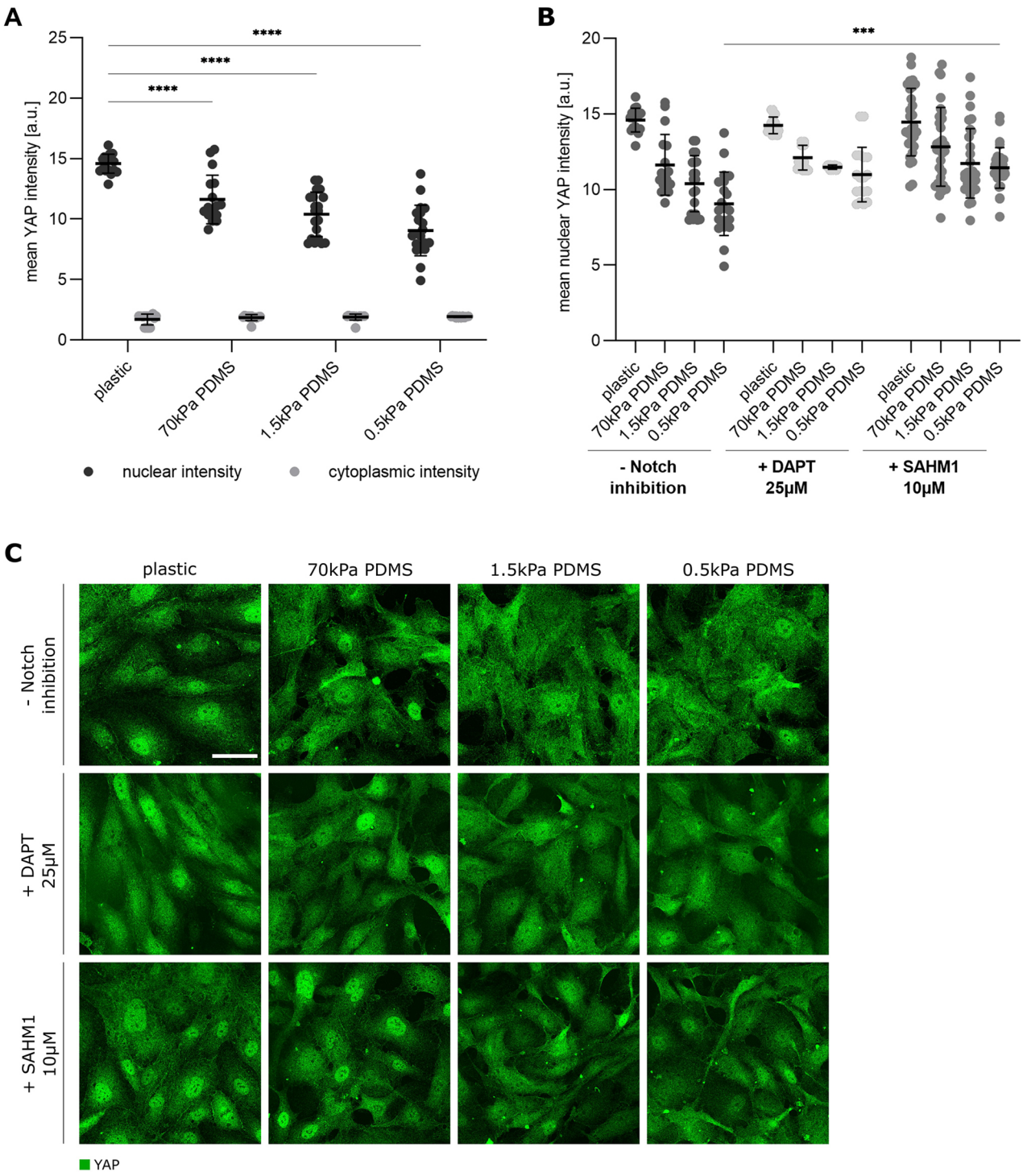

Fig. 3. Nuclear YAP intensity is reduced on softer substrates but is only marginally affected by Notch inhibition. (A) Nuclear and cytoplasmic YAP intensities. HUVEC cells were seeded on varying substrate stiffness, as indicated, and were stained for YAP. Intensities were analyzed using the Intensity Ratio Nuclei Cytoplasm Tool plugin for ImageJ and are presented as the mean±s.d. of ≥240 cells derived from three independent experiments (a.u., arbitrary units). ****P<0.0001 (two-way ANOVA followed by Tukey's multiple comparison test). (B) Nuclear YAP intensities with and without Notch inhibition. HUVEC cells were seeded on varying substrate stiffness and treated with 25 µM DAPT or 10 µM SAHM1 for 24 h, as indicated, before being stained for YAP. Intensities were analyzed using the Intensity Ratio Nuclei Cytoplasm Tool plugin for ImageJ and are presented as the mean±s.d. nuclear intensity of ≥240 untreated and treated cells derived from three independent experiments. ***P<0.001 (two-way ANOVA followed by Tukey's multiple comparison test). (C) Representative images of immunofluorescence staining of HUVEC cells on varying substrate stiffness, with or without treatment with DAPT or SAHM1, as indicated. YAP staining is shown in green. Scale bar: 50 µm.

(Fig. 6C), where the rhDll4 coat is evenly distributed on all substrates (Fig. S1). In contrast, no change in reporter gene activity was evaluated on the substrates without Notch activation (collagen G coat). Thus, cell–cell contacts contribute to Notch activity but are not necessary for the mechanomodulation of Notch signaling in this setting.

Journal of Cell Science (2023) 136, jcs260442. doi:10.1242/jcs.260442

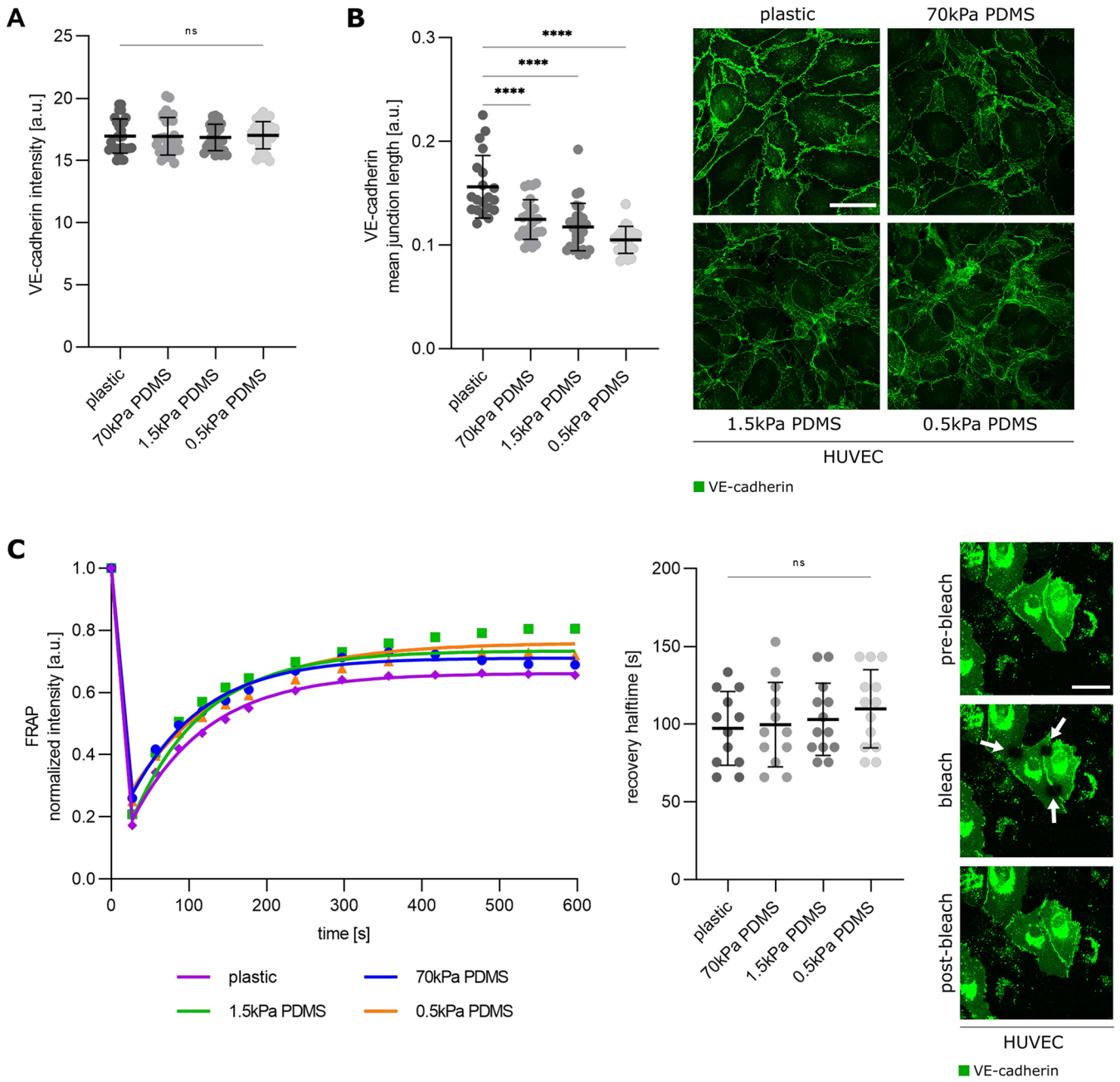

Fig. 4. Softer substrates change VE-cadherin junction morphology but not VE-cadherin levels or its mobility. (A) VE-cadherin intensity (a.u., arbitrary units) at the cell–cell contacts in HUVEC cells, quantified after distinction of VE-cadherin structures using segmentation. (B) VE-cadherin junction analysis in HUVECs, quantified by skeletonizing and skeleton analysis. For A and B, cells were seeded on varying substrate stiffness and were stained for VE-cadherin. Intensity and junction analyses are presented as the mean±s.d. of ≥240 cells derived from three independent experiments. ****P<0.0001; ns, not significant (one-way ANOVA followed by Tukey's multiple comparison test). Representative images of immunofluorescence staining of HUVECs on the indicated substrates are shown on the right of panel B, with VE-cadherin in green. Scale bar 50 µm. (C) Analysis of VE-cadherin mobility at the cell–cell border in HUVECs using a FRAP assay. Cells were transiently transfected with mCitrine-VE-Cadherin-N-10 plasmid and seeded on varying substrate stiffness, as indicated. FRAP was conducted using the Leica photo bleaching module. VE-cadherin recovery is plotted over time (left panel; representative recovery curves are shown) and quantified as recovery half time (middle panel). Recovery half times are presented as mean±s.d. of ≥12 cells with one to three ROIs derived from three independent experiments. ns, not significant (one-way ANOVA followed by Tukey's multiple comparison test). The intensities of the ROIs at the various measurement points were detected and plotted as a function of time; recovery half times were determined from the recovery curves. Representative images of the three FRAP steps and the typical location of ROIs (arrows) are shown on the right. Citrine-coupled VE-cadherin is shown in green. Scale bar: 50 µm. Please note that transfection efficiency was ∼30%. Only the mCitrine-VE-Cadherin-N-10-expressing cells are visible in the images.

DISCUSSION

The Notch signaling pathway plays multiple and crucial roles in developmental and pathological processes (Artavanis-Tsakonas et al., 1999; Aster et al., 2017; Bray, 2016). Many of these scenarios are related to changes in the composition and the biomechanical features of the ECM. During angiogenesis, the Notch signaling pathway regulates cell fate decisions such as migration, proliferation and differentiation, which are essential for vascular development

Journal of Cell Science (2023) 136, jcs260442. doi:10.1242/jcs.260442

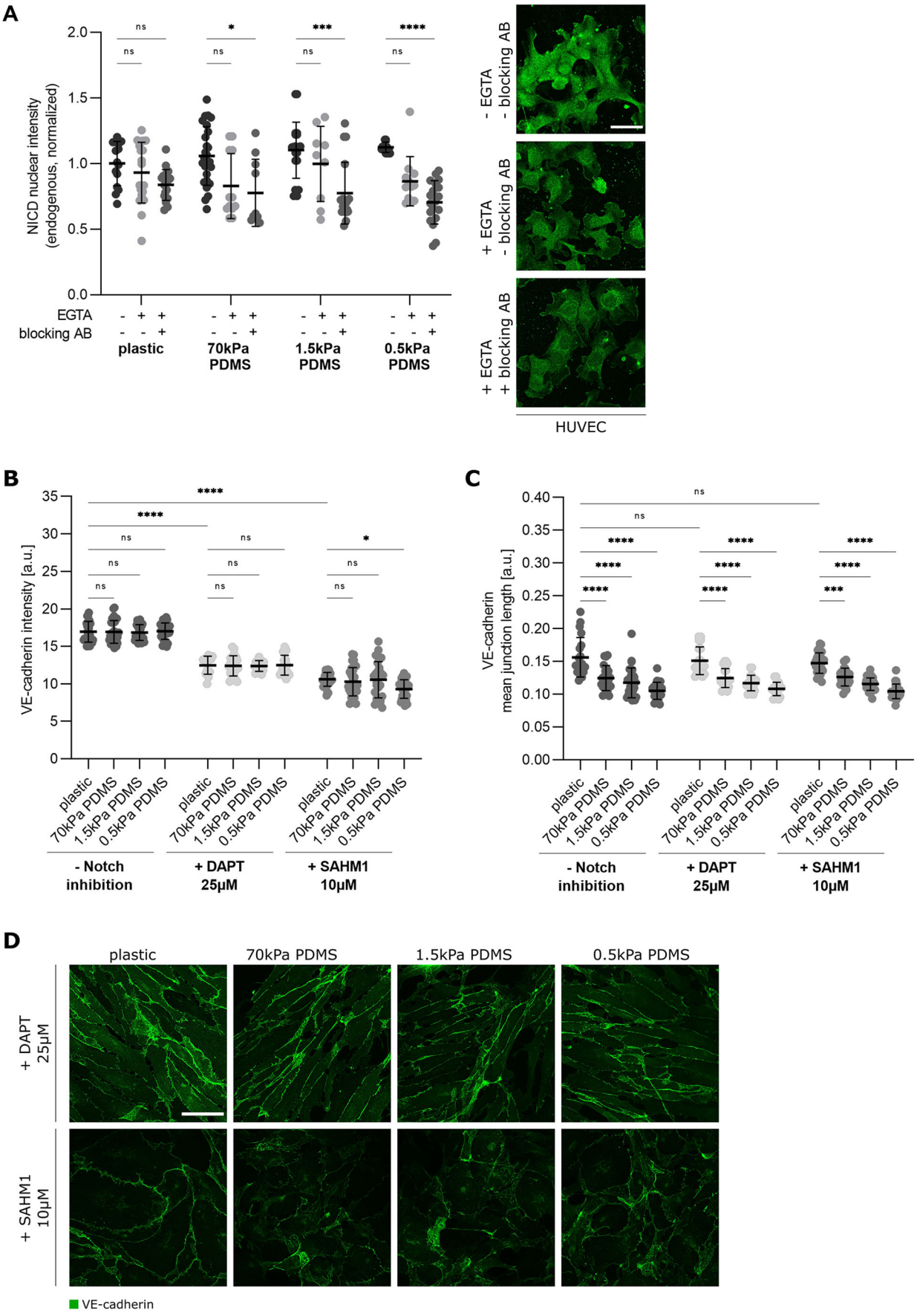

Fig. 5. See next page for legend.

Journal of Cell Science (2023) 136, jcs260442. doi:10.1242/jcs.260442

Fig. 5. Notch and VE-cadherin influence each other – basal Notch activity is reduced by VE-cadherin blocking and VE-cadherin intensity is decreased by Notch inhibition. (A) Endogenous nuclear NICD intensity in HUVECs after cell–cell contact inhibition. Cells were seeded on substrates of varying stiffness, as indicated, without further activation of the Notch signaling pathway. Cells were either untreated, treated with EGTA for 30 min, or treated with EGTA for 30 min then washed and incubated with VE-cadherin-blocking antibody (blocking AB) for a further 30 min before staining for NICD. Left: intensities were analyzed using the Intensity Ratio Nuclei Cytoplasm Tool plugin for ImageJ then normalized to the intensities on plastic without any treatment. Data are presented as mean±s.d. of ≥240 cells derived from three independent experiments. *P>0.1; ***P<0.001; ****P<0.0001; ns, not significant (two-way ANOVA followed by Tukey's multiple comparison test). Right: representative images of HUVEC cells on 0.5 kPa PDMS after immunofluorescence staining, with NICD in green. Scale bar: 50 µm. (B,C) VE-cadherin intensity and junction analysis in HUVECs with and without Notch inhibition. Cells were seeded on varying substrate stiffness and treated with 25 µM DAPT or 10 µM SAHM1 for 24 h, as indicated, before being stained for VE-cadherin. (B) VE-cadherin intensity (a.u., arbitrary units) presented as mean±s.d. of ≥240 cells derived from three independent experiments. *P<0.1; ****P<0.0001; ns, not significant (one-way ANOVA followed by Tukey's multiple comparison test). (C) VE-cadherin mean junction length, evaluated after segmentation, skeletonizing and skeleton analysis. Data are displayed as mean±s.d. of ≥240 cells. ***P<0.001; ****P<0.0001; ns, not significant (one-way ANOVA followed by Tukey's multiple comparison test). (D) Representative images of HUVECs on plastic and PDMS substrates with addition of DAPT or SAHM1, as indicated, and after immunofluorescence staining for VE-cadherin (green). Scale bar: 50 µm.

and angiogenesis (Merk et al., 2016; Takeshita et al., 2007). Endothelial Notch signaling can be activated by VEGFA, and at the same time VEGFA controls matrix composition, causing local ECM softening or stiffening (Estrach et al., 2011; Stepanova et al., 2021). Previous studies on biophysical aspects of Notch signaling have focused on a pulling force exerted by the bound receptor (Sprinzak and Blacklow, 2021) that is a prerequisite for Notch receptor cleavage. To date, however, little is known about whether the Notch signaling pathway is modulated by substrate stiffness. To address this question, we used an endothelial cell model based on synthetic PDMS substrates with tunable stiffness. The substrates we used cover the physiological stiffness ranges of soft organ tissues such as breast, brain or liver (0.5 kPa); of endothelial tissue or pathological hepatoma tissue (1.5 kPa); of firmer tissue such as skin, but also pathological cervical cancer tissue (70 kPa); and of very firm tissue such as bone structures (plastic) (Cui et al., 2017; Zanotelli and Reinhart-King, 2018).

Interestingly, nuclear NICD localization, transcriptional activity of Notch, and mRNA expression of Notch receptor and target genes were found to increase with decreasing substrate stiffness. This phenomenon occurs irrespective of whether Notch activation was achieved by surface-bound ligand (rhDll4) or Dll4-overexpressing sender cells (Fig. 1).

Endothelial cells sense changes of matrix properties via cell–matrix adhesion proteins, such as integrin β1 (Estrach et al., 2011; Fischer et al., 2009), which also plays a crucial role in regulating cellular adhesion to enable migration and proliferation (Estrach et al., 2011; Matsuo et al., 2021). Since integrins have been previously located both upstream (Rallis et al., 2010) and downstream of Notch in signaling pathways (Hodkinson et al., 2007), we first investigated this issue. For integrin β1, it has already been shown that the overall levels do not change with different substrate stiffnesses, but that the active state of integrin β1 increases on softer substrates (Du et al., 2011). We confirm these observations in our model. Furthermore, our data show that cell–matrix adhesion is directly influenced by the Notch signaling pathway. Notch inhibition by DAPT or SAHM1 treatment significantly reduced the integrin β1 intensity of the activated form, although substrate-dependent activation was further observed (Fig. 2). These results corroborate the findings of Hodkinson et al., which show that Notch1, through NICD cleavage and subsequent R-Ras binding, can induce a conformational change in the surface-bound integrin from a low-affinity state to a high-affinity state, mobilizing the active form (Hodkinson et al., 2007). This clearly positions integrins downstream of Notch. Despite Notch inhibition, a continuous increase in integrin β1 levels on softer substrates can be observed; however, this occurs on a much lower level (Fig. 2). Thus, either pharmacological Notch inhibition was not complete or integrin activity is additionally influenced by substrate stiffness via an alternative pathway.

The role of YAP as a mechanotransducer and the related mechanosensitivity of the YAP–TAZ signaling pathway are well known and studied. Upon YAP activation – for example, by higher ECM rigidly or substrate stiffness – YAP and TAZ are not phosphorylated and can thus be relocated from the cytoplasm to the nucleus, where binding to a transcription factor regulates genes necessary for cell migration and proliferation (Das et al., 2016; Nukuda et al., 2015). Accordingly, we investigated, how the YAP–TAZ pathway relates to stiffness-modulated Notch signaling. As expected, YAP activity decreased with lower stiffness of the substrate (Fig. 3). It has been previously shown that activation of YAP reduces Notch signaling by repression of the ligand Dll4, whereas knockdown of YAP increases Dll4 (Yasuda et al., 2019). However, this mechanism is not sufficient to explain the correlation between substrate stiffness and Notch activity in our model because we examined Notch activation after co-culture with a stably overexpressing cell line. Additionally, increased activity of Notch with lower stiffness was also observed after activation by rhDll4, which is independent of YAP activity. There also seems to be no feedback loop between Notch and YAP translocation, since neither DAPT nor SAHM1 treatment altered stiffness dependence of YAP translocation to the nucleus (Fig. 3). However, we cannot exclude concomitant activation of YAP and Notch on a transcriptional level, which has been described previously (Totaro et al., 2018).

In addition to the effect on cell–matrix adhesions, a stiffness effect has already been established for cell–cell contacts. On stiffer substrates, VE-cadherin junctions are wider and discontinuous, whereas on soft substrates they are narrower but continuous (Bordeleau et al., 2017). We have corroborated this finding by analyzing VE-cadherin patterns through mean branch length evaluation. The VE-cadherin junctions on plastic show a branched, comb-like structure with longer branches, in contrast to the narrower junctions observed on softer substrates, which have shorter branches and appear more distinct and continuous (Fig. 4). A role for cadherins in the regulation of the Notch signaling pathway has previously been described by Kwak et al., who demonstrated that cadherin-based adherens junctions control Notch–γ-secretase interactions (Kwak et al., 2022). In this context, the changes in VE-cadherin junctions on the soft substrates could be related to the increased Notch activity. However, it should be noted that the VE-cadherin patterns on the changing substrate stiffnesses do not affect the intensity level or VE-cadherin trafficking (Fig. 4). Furthermore, Notch signaling is regulated by the cell–cell contact area (Shaya et al., 2017; Totaro et al., 2018), as signaling is directly linked to the contact area of two interacting cells (Shaya et al., 2017). By destabilizing and blocking the cell–cell contacts, we have confirmed that, as expected, Notch activity is reduced. This effect is, however,

Journal of Cell Science (2023) 136, jcs260442. doi:10.1242/jcs.260442

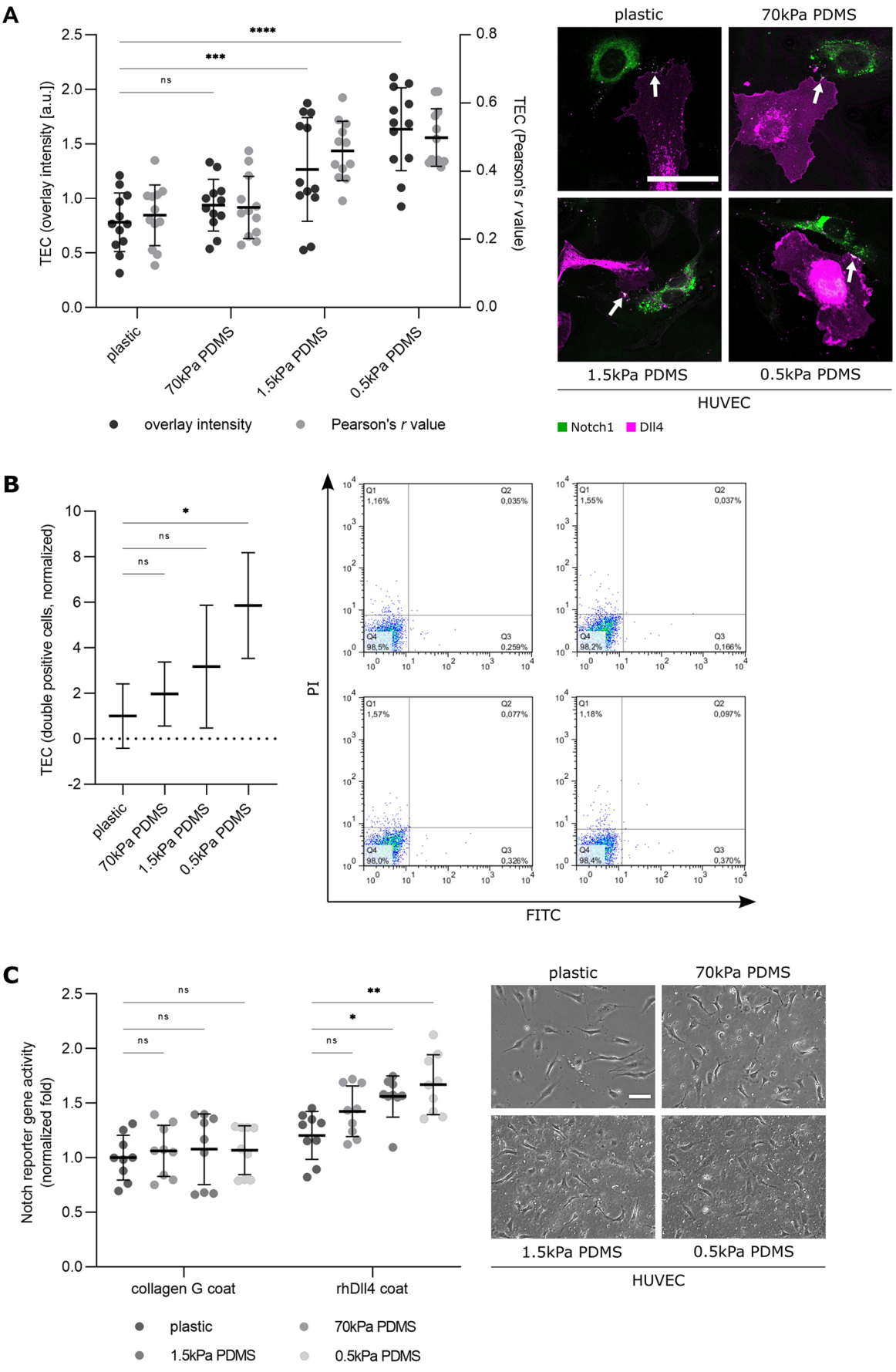

Fig. 6. See next page for legend.

Journal of Cell Science (2023) 136, jcs260442. doi:10.1242/jcs.260442

Fig. 6. Trans-endocytosis is increased on softer substrates, and cell–cell contacts are dispensable for Notch activation with rhDll4. (A) Left: overlay intensity (a.u., arbitrary units) and Pearson's *r* value in areas of Notch receptor–ligand interactions in the signal-sending cell (Dll4-expressing cell). HUVEC cells were transfected separately with a Citrine-coupled Notch1 extracellular domain plasmid or an mCherry-coupled Dll4 plasmid. Trans-endocytosis (TEC) was quantified at receptor–ligand interactions in ≥12 signal-sending cells per substrate condition in three independent experiments. Data are presented as mean±s.d. ***P<0.001; ****P<0.0001; ns, not significant (two-way ANOVA with Tukey's multiple comparison test). Right: representative images of TEC on the indicated substrates are shown. Notch1-expressing Notch receiver cells are shown in green, Dll4-expressing Notch sender cells are shown in magenta. Overlay areas are indicated by the white arrows. Scale bar: 50 µm. (B) Normalized percentage of cells positive for both Notch1–Citrine and Dll4–mCherry (double-positive cells). HUVEC cells were transfected separately with a Citrine-coupled Notch1 plasmid and an mCherry-coupled Dll4 plasmid. Trans-endocytosis was quantified by flow cytometry. Percentages of cells showing a signal in both the FITC channel (Notch1–Citrine) and PI channel (Dll4–mCherry) were normalized to the percentage for cells on the plastic substrate and are summarized on the left (mean±s.d.; data derived from three independent experiments with 10,000 analyzed cells in each run). *P<0.1; ns, not significant (one-way ANOVA followed by Tukey's multiple comparison test). Representative dot plots of the flow cytometry are shown on the right (Q1: $FITC^-$, PI^+; Q2: $FITC^+$, PI^+; Q3: $FITC^+$, PI^-; Q4: $FITC^-$, PI^-), with the percentage of cells in each quadrant indicated. (C) Normalized reporter gene activity in non-confluent HUVEC cells with and without Notch activation via a rhDll4 coat, determined by detection of cellular luciferase levels under control of the TP1-Luc Notch reporter. Data were normalized to cells on plastic without Notch activation (with a collagen G coat). Reporter gene assays were performed for cells on substrates with different stiffnesses, as indicated, and the data are presented as mean±s.d. of three independent experiments, each with triplicates. *P<0.1; **P<0.01; ns, not significant (two-way ANOVA followed by Tukey's multiple comparison test). Representative images of the cell density are shown on the right. The PDMS matrix becomes cloudier as the stiffness decreases, making the cells more difficult to identify. Please note that transfection efficiency in HUVECs was ∼30%. Scale bar: 50 µm.

independent of substrate stiffness (Fig. 5). In this context, it should be noted that the Notch receptor has a Ca^{2+} dependency, which means that the use of EGTA to destabilize the cell–cell contacts could also destabilize the receptor, leading to Notch cleavage and activation (Rand et al., 2000; Tremblay et al., 2013). Thus, this result should be interpreted with care. Blocking the Notch signaling pathway leads to a uniform decline of VE-cadherin on all substrates. The change in junctional patterns due to variation of stiffness is not influenced by DAPT treatment (Fig. 5). These findings argue against an upstream role of VE-cadherin in stiffness regulation of Notch signaling.

Endocytosis of the Notch ligand into the signal-sending cell after binding to the receptor can, on one hand, counteract the accumulation of Notch receptor on the surface of the signal-receiving cell and, on the other hand, serve primarily for receptor activation (Antfolk et al., 2017; Shergill et al., 2012). During trans-endocytosis, the extracellular part of the Notch receptor bound to the Notch ligand is pulled into the ligand-presenting cell, thus releasing the intracellular part of the receptor (the activated form), which can be detached from the membrane in a further cleavage event (Nichols et al., 2007). Our results from the trans-endocytosis assay on the different substrates show that trans-endocytosis is significantly enhanced on soft substrates, which is consistent with the enhanced Notch activity on softer substrates. A stiffness effect on the general endocytosis can be excluded. Taken together, these observations demonstrate a mechanosensitivity of the Notch signaling pathway that may in part be due to trans-endocytosis. Interestingly, however, we find that activation of the Notch signaling pathway in a cell–cell contact-independent manner – by using rhDll4 as a stimulus for subconfluent single cells – still responds to substrate stiffness. Whereas a mechanical aspect of Notch pathway activation following interaction with a ligand-presenting cell – namely the pulling movement of the ligand into the sender cells – has previously been established, the mechanism of mechanosensitivity of the Notch pathway after rhDll4 activation, and thus without trans-endocytosis and pulling movement, is to date unknown and is based on a different mode of action or mechanical force.

These findings might be of importance to better understand the effects of matrix remodeling on endothelial cell behavior and adjustment of their gene expression (Shamloo et al., 2016; Stepanova et al., 2021). Matrix remodeling increases the elasticity of the matrix and thus decreases the stiffness of the ECM (Perfahl et al., 2017; Shamloo et al., 2016), thus triggering a feedback loop. With Notch being one of the main regulators of endothelial cell fate decisions as well as being the key mediator of angiogenesis by controlling tip and stalk cell differentiation (Antfolk et al., 2017; Fernandez-Chacon et al., 2021), our results provide further insights into the consequences of normal and pathological matrix changes for endothelial behavior during angiogenic sprouting in development and maintenance.

MATERIALS AND METHODS

Cell culture and co-cultures

Human umbilical vein endothelial cells (HUVECs) were obtained from Promocell (Heidelberg, Germany), Human microvascular endothelial cells (HMECs) were a gift from Dr Guido Jürgenliemk (University of Regensburg, Germany). Cells were cultured in ECGM medium (PELO Biotech, Planegg, Germany) including the supplement kit, 10% heat-inactivated fetal calf serum (FCS; PAA Laboratories GmbH, Pasching, Austria), 250 µg/ml amphotericin B and 10,000 U/ml penicillin-streptomycin (PAN Biotech, Aidenbach, Germany) at 37°C and 5% CO_2 under constant humidity. Cells were maintained until passage six for the experiments.

Mouse cardiac endothelial cells (MCECs) were a gift from Andreas Fischer (DKFZ, Heidelberg, Germany) and were maintained in DMEM medium supplemented with 10% FCS (PAA Laboratories GmbH) and 200 mM L-glutamine (Thermo Fisher Scientific, Waltham, MA, USA). Two MCEC cell lines were used: a wild-type cell line (MCEC-WT) as well as a cell line overexpressing Dll4 coupled to an mCherry reporter (MCEC-Dll4–mCherry). At confluence, cells were split and cultivated with continuous passage.

Unless stated otherwise, all experiments were performed using confluent cultures. HUVEC–MCEC co-cultures were suspended in ECGM medium; MCEC–MCEC co-cultures were suspended in DMEM medium.

Generation of stable cell lines

The generation of MCEC TetR-TO-Dll4-mCherry (MCEC-Dll4–mCherry) was performed in two steps. First, MCEC-TetR cells were generated by stable transfection of the pcDNA6-TR-Blast plasmid (gifted from the Bjorkman lab, Division of Biology and Biological Engineering, California Institute of Technology, Pasadena, CA, USA) and selection of single clones using 10 µg/ml blasticidin (H-1012-PBS; A.G. Scientific Inc., San Diego, CA, USA). Then, MCEC-TetR cells were transfected with the pcDNA5-TO-hDll4-mCherry plasmid (Sprinzak et al., 2010) and were placed under another selection with 250 µg/ml hygromycin (B-1247-SOL; A.G. Scientific Inc.). Single colonies were picked and tested for fluorescence under conditions with and without 100 µg/ml doxycycline (Sigma-Aldrich, St Louis, MO, USA).

Coating of substrate surfaces

To ensure uniform adhesion, all applied surfaces and substrates were coated with collagen G from bovine skin (10 µg/ml in PBS; 50104, MATRIX BioScience GmbH, Mörlenbach, Germany) before cell seeding. The coating

solution was incubated at 37°C, 5% CO_2 for 30 min and then aspirated for cell seeding.

For coating with rhDll4, the rhDll4 (R&D Systems, Minneapolis, MN, USA) was reconstituted at 200 µg/ml with pure PBS and used at working concentrations of 1 µg/ml. The rhDll4 solution was incubated overnight at 4°C and, for temperature equilibration, for 1 h at room temperature on the different substrates before it was aspirated for cell seeding.

Polydimethylsiloxane gels

PDMS substrates were prepared using the Sylgard™ 184 silicone elastomer kit (Dow Corning, Midland, MI, USA). PDMS base was mixed with a ratio of 10%, 2% or 1.3% curing agent and was transferred to 8-well or 2-well µ-slides from ibidi (Martinsried, Germany). Gels were degassed in a desiccator for 10–15 min and polymerized in a compartment drier at 60°C for 20 h, resulting in substrate stiffnesses of 70 kPa, 1.5 kPa and 0.5 kPa. PDMS substrates were hydrophilized with oxygen plasma at 0.3 mbar for 3 min using the Zepto plasma system (Diener electronic GmbH & Co. KG, Ebhausen, Germany). Stiffnesses were determined after hydrophilization by rheometric measurements using the Modular Compact Rheometer MCR 100 (Physica, Stuttgart, Germany).

Cell proliferation

Cells were seeded at 250,000 cells/well in 6-well plates on plastic and PDMS substrates coated with collagen G in PBS. After incubation of 24 h and 48 h, cells were stained with Crystal Violet and lysed in sodium citrate buffer. For detection, 100 µl/well of the solution was transferred to a 96-well plate, and the absorbance was measured at 595 nm. All cell proliferation assays were carried out in triplicate.

Cell viability

Cytotoxicity of the Notch inhibitors SAHM1 and DAPT on endothelial cells was assessed using the CellTiter-Blue cell viability assay (Promega, Madison, WI, USA). Cells were seeded at 20,000 cells/well, incubated for 24 h and treated with the inhibitors as indicated for another 24 h. CellTiter-Blue Reagent was added in a ratio of 1:5. Fluorescence intensity was measured using the SpectraFluor Plus plate reader (Tecan, Männedorf, Switzerland) at 550/595 nm. Fluorescence intensity is proportional to the cell number. Cells without treatment were used as negative controls. All experiments were conducted in triplicate.

Plasmids and transfections

The TP1-Luc construct was first published by Minoguchi et al. (Minoguchi et al., 1997). pRL-SV40P Renilla was obtained from Addgene (Addgene plasmid 27163; deposited by Ron Prywes). The pcDNA3-hN1-citrine plasmid was constructed from pcdna3-hNECD-G4esn-cit, described in previous work (Sprinzak et al., 2010). The G4esn was replaced with the full length of human Notch1, leaving only the extracellular domain. pcDNA5-TO-hDll4-mCherry has been described previously (Sprinzak et al., 2010). mCitrine-VE-Cadherin-N-10 was obtained from Addgene (Addgene plasmid 56319; deposited by Michael Davidson; RRID: Addgene_56319).

HUVECs were transfected transiently using either the Targefect-HUVEC™ transfection kit (Targeting Systems, El Cajon, CA, USA) or the Cell Line Nucleofector™ Kit V with the program A-034 (Lonza Group AG, Basel, Switzerland) according to manufacturers' protocols. MCECs were transiently transfected with the FuGENE® Transfection Regent (Promega) following the manufacturer's instructions. Transfected cells were incubated for 24 h before further assays or evaluations were applied. With HUVECs, we routinely reached transfection efficiencies of ∼30%.

Reporter gene assay

Notch-responsive dual luciferase reporter assays were performed 24 h subsequent to co-transfection of endothelial cells with the CSL-binding plasmid TP1-Luc and Renilla luciferase. Firefly luciferase and Renilla luciferase vector levels were applied in a ratio of 10:1. Using the Dual-Luciferase® Reporter Assay System (Promega) and the Orion II microplate luminometer equipped with Simplicity analysis software (Berthold Technologies, Bad Wildbad, Germany), luciferase levels of triplicates per condition were determined. Firefly luciferase relative light units (RLUs) were normalized to the Renilla luciferase control. This approach compensates for changes of transfection efficiencies between experiments or potential cell death.

Trans-endocytosis assay

Cells grown to 80% confluency (HUVECs or MCEC-WTs) were transiently transfected separately with the plasmids pcDNA3-hN1-citrine and pcDNA5-TO-hDll4-mCherry and incubated on plastic for 24 h at 37°C under 5% CO_2. Cells were then washed, detached and reseeded together in a co-culture ratio of 1:1. Doxycycline was added during reseeding at a concentration of 100 ng/ml for activation of Dll4–mCherry expression and incubated for 6 h at 37°C under 5% CO_2. For visualization of the trans-endocytosis by confocal microscopy, co-cultures were fixed with 4% methanol-free formaldehyde (Thermo Fisher Scientific) in PBS for 10 min. Samples were washed twice with PBS and sealed with FluorSave mounting medium. Quantification was performed by analysis of colocalized areas of Notch extracellular domain and Dll4 in the signal-sending cell (Dll4-expressing cell) by defining regions of interest (ROIs) and measuring their intensity using ImageJ. For the detection of trans-endocytosis by flow cytometry, the cells were detached, collected by centrifugation, and washed and resuspended in ice-cold PBS. Flow cytometry was performed on a BD FACS Canto II (BD Biosciences, Franklin Lakes, NJ, USA). Fluorescence intensity of Notch1–Citrine (plasmid) was analyzed using the FITC channel, and fluorescence intensity of Dll4–mCherry (plasmid) was analyzed using the PI channel. 10,000 cells were analyzed per run. Data were evaluated using the FlowJo 7.6 software.

Transferrin endocytosis assay

Cells grown to 100% confluence were washed once with PBS including Ca^{2+} and Mg^{2+} (PBS^{+}; 0.25 mM $MgCl_2$ and 0.5 mM $CaCl_2$) and incubated for 10 min with 5 µg/ml Transferrin, Alexa Fluor 488 conjugate (Life Technologies, Carlsbad, CA) at 37°C under 5% CO_2. Cells were washed once with room temperature acid-wash medium (150 mM NaCl, 1 mM $MgCl_2$, 0.125 mM $CaCl_2$, 0.1 M glycine, pH 2.5) and then fixed with 4% methanol-free formaldehyde (Thermo Fisher Scientific) in PBS for 10 min. Samples were washed twice with PBS and sealed with FluorSave mounting medium. Transferrin uptake was visualized by confocal microscopy.

Antibodies, compounds and staining reagents

The following primary antibodies were used in this study: anti-cleaved Notch1 (Val1744; rabbit mAb IgG, 4147; Cell Signaling Technology, Danvers, MA, USA), anti-integrin β1 (rabbit pAb, 4706; Cell Signaling Technology), anti-integrin beta 1 (12G10; mouse mAb IgG_1; ab30394, Abcam, Cambridge, UK), anti-YAP (D8H1X; XP® rabbit mAb IgG; 14074, Cell Signaling Technology) and anti-VE-Cadherin (rabbit pAb; 2158, Cell Signaling Technology). All primary antibodies were diluted 1:200 for application. The following secondary antibodies were applied in this study: Alexa Fluor 488-conjugated goat anti-mouse IgG (H+L), A-11001; Alexa Fluor 488-conjugated goat anti-rabbit IgG (H+L), A-11008; and Alexa Fluor 647-conjugated chicken anti-rabbit IgG (H+L), A-21443 (all from Thermo Fisher Scientific). All secondary antibodies were diluted 1:400 for application.

DAPT was purchased from Sigma-Aldrich (D5942), dissolved in DMSO to a stock concentration of 10 mM and used at a working concentration of 25 µM. DMSO controls were performed with the appropriate DMSO concentrations. SAHM1 was obtained from R&D Systems (6477/1), dissolved in H_2O to a stock concentration of 1 mg/ml and used at a working concentration of 10 µM. EGTA was purchased from Sigma-Aldrich (E4378) and applied at 5 mM. The VE-cadherin-blocking antibody clone BV6 (MABT134) was obtained from Merck Millipore (Darmstadt, Germany) and was diluted 1:10 for use (50 µg/ml). Hoechst 33342 was purchased from Sigma-Aldrich (B2261), dissolved in PBS and applied at a final concentration of 10 µg/ml. FluorSave™

Reagent was purchased from Merck Millipore (345789; Darmstadt, Germany).

Immunofluorescence staining

Cells were washed once with PBS^+ and were fixed with 4% methanol-free formaldehyde (Thermo Fisher Scientific) in PBS for 10 min. Fixation was followed by a brief washing with PBS and cell permeabilization with 0.1% Triton X-100 in PBS for 10 min. After another brief washing with PBS, nonspecific binding sites were blocked with 5% BSA (Roth, Karlsruhe, Germany) in PBS for 60 min. Cells were then incubated with the primary antibody diluted in PBS with 1% BSA (1:200) overnight at 4°C. Next, samples were washed 3×10 min with 1% BSA in PBS, then incubated with the secondary antibody (1:400) and Hoechst 33342 (1:100) for nuclear counterstain, again diluted in PBS with 1% BSA for 1 h at room temperature. Cells were washed again 2×10 min with 1% BSA in PBS and once for 10 min with PBS, and were sealed with FluorSave mounting medium.

Laser scanning confocal microscopy

Confocal images were taken with a Leica TCS SP8 microscope equipped with an HC PL APO CS2 63×/1.4 oil objective and photomultiplier (PMT) or HyD detectors, using the LAS X core software. In sequential scanning mode, two frames were acquired for every channel with a scanning speed of 400 Hz, and the pinhole size was set to 1.0 airy units. The following excitation laser lines were applied: 405 nm, 488 nm and 647 nm.

Fluorescence recovery after photobleaching

HUVECs were transiently transfected with mCitrine-VE-Cadherin-N-10, seeded directly on different substrates (plastic and PDMS) and incubated for 24 h at 37°C under 5% CO_2. The FRAP assay was conducted with the Leica TCS SP8 SMD microscope with the HC PL APO CS2 63×/1.4 NA oil objective and the heating and gas incubation system from OCO Lab (Naples, Italy) ensuring constant 37°C under 5% CO_2 and 80% humidity. Using the LAS X Core Software, the FRAP settings were adjusted to one pre-bleach iteration, 20 bleach iterations, five post-bleach iterations with 30 s intervals and seven with 60 s intervals. Images were taken with a pinhole size adjusted to 1.0 airy units and a scanning speed of 400 Hz. The 488 nm (argon) laser line and the PMT detector were applied.

Reverse transcription and quantitative real-time PCR

RNA was isolated from cell samples using the RNeasy Mini Kit (Qiagen, Venlo, Germany) according to the manufacturer's instructions. After determining the yield with a NanoDrop spectrophotometer (Thermo Fisher Scientific), 1250 ng of the mRNA was reverse-transcribed using the High-Capacity cDNA Reverse Transcription Kit (Applied Biosystems, Waltham, MA, USA) as described by the manufacturer. RT-qPCR experiments were performed using an Applied Biosystems® QuantStudio™ 3 Real-Time PCR System (Thermo Fisher Scientific) with standard procedures. SYBR™ Green Master Mix (Thermo Fisher Scientific) was used for cDNA amplification and detection. GAPDH served as a housekeeping gene. The following primers were purchased from Metabion (Planegg, Germany): *Dll4* forward, 5′-CTGCGAGAAGAAGTGGACAGG-3′; *Dll4* reverse, 5′-ACAGTCGCTGACGTGGAGTTCA-3′; *Jag1* forward, 5′-TGCTACAA-CCGTGCCAGTGACT-3′; *Jag1* reverse, 5′-TCAGGTGTGTCGTTGGA-AGCCA-3′; *Hey1* forward, 5′-TGTCTGAGCTGAGAAGGCTGGT-3′; *Hey1* reverse, 5′-TTCAGGTGATCCACGGTCATCTG-3′. Data were evaluated using the ΔΔCT method, as described previously (Fleige et al., 2006).

Data analysis and statistics

All confocal images were analyzed using ImageJ version 1.53c (NIH, Bethesda, MD, USA). Only two-dimensional images were evaluated. Pearson's *r* coefficients were determined using the Coloc2 plugin for ImageJ. Nuclear:cytoplasmic intensity ratios were evaluated with the Intensity Ratio Nuclei Cytoplasm Tool plugin (RRID: SCR_018573) for ImageJ. Expression patterns were determined by segmentation and skeletonizing of the images, as described previously (Arganda-Carreras et al., 2010, 2017).

All data were derived from three independent experiments and are represented as the mean±s.d. In the case of confluent cell layers, entire image sections were analyzed unless the separate analysis of individual cells is described. An image section of confluent cells contained ≥20 cells. Statistical analysis were performed as ordinary one-way or two-way ANOVA with Tukey's multiple comparison tests using GraphPad Prism 9.2.0 (sample size and variance were homogenous).

Competing interests

The authors declare no competing or financial interests.

Author contributions

Conceptualization: M.K., D.S., S.Z.; Methodology: R.M.; Investigation: M.K.; Resources: R.M., D.S., A.M.V.; Writing - original draft: M.K.; Writing - review & editing: D.S., A.M.V., S.Z.; Visualization: M.K.; Supervision: D.S., A.M.V., S.Z.; Project administration: S.Z.; Funding acquisition: S.Z.

Funding

This project was funded by the Deutsche Forschungsgemeinschaft, project ID 201269156 – SFB 1032 (project B8). D.S. acknowledges the support of the European Research Council (ERC) under the European Union's Horizon 2020 research and innovation programme (grant agreement 682161). Open Access funding provided by Deutsche Forschungsgemeinschaft. Deposited in PMC for immediate release.

Data availability

All relevant data can be found within the article and its supplementary information.

Peer review history

The peer review history is available online at https://journals.biologists.com/jcs/lookup/doi/10.1242/jcs.260442.reviewer-comments.pdf

References

Andrawes, M. B., Xu, X., Liu, H., Ficarro, S. B., Marto, J. A., Aster, J. C. and Blacklow, S. C. (2013). Intrinsic selectivity of Notch 1 for Delta-like 4 over Delta-like 1. *J. Biol. Chem.* **288**, 25477-25489. doi:10.1074/jbc.M113.454850

Antfolk, D., Sjoqvist, M., Cheng, F., Isoniemi, K., Duran, C. L., Rivero-Muller, A., Antila, C., Niemi, R., Landor, S., Bouten, C. V. C. et al. (2017). Selective regulation of Notch ligands during angiogenesis is mediated by vimentin. *Proc. Natl. Acad. Sci. USA* **114**, E4574-E4581. doi:10.1073/pnas.1703057114

Arganda-Carreras, I., Fernandez-Gonzalez, R., Munoz-Barrutia, A. and Ortiz-De-Solorzano, C. (2010). 3D reconstruction of histological sections: Application to mammary gland tissue. *Microsc. Res. Tech.* **73**, 1019-1029. doi:10.1002/jemt.20829

Arganda-Carreras, I., Kaynig, V., Rueden, C., Eliceiri, K. W., Schindelin, J., Cardona, A. and Sebastian Seung, H. (2017). Trainable Weka Segmentation: a machine learning tool for microscopy pixel classification. *Bioinformatics* **33**, 2424-2426. doi:10.1093/bioinformatics/btx180

Artavanis-Tsakonas, S., Rand, M. D. and Lake, R. J. (1999). Notch signaling: cell fate control and signal integration in development. *Science* **284**, 770-776. doi:10.1126/science.284.5415.770

Aster, J. C., Pear, W. S. and Blacklow, S. C. (2017). The varied roles of notch in cancer. *Annu. Rev. Pathol.* **12**, 245-275. doi:10.1146/annurev-pathol-052016-100127

Boareto, M., Jolly, M. K., Lu, M., Onuchic, J. N., Clementi, C. and Ben-Jacob, E. (2015). Jagged-Delta asymmetry in Notch signaling can give rise to a Sender/Receiver hybrid phenotype. *Proc. Natl. Acad. Sci. USA* **112**, E402-E409.

Bordeleau, F., Mason, B. N., Lollis, E. M., Mazzola, M., Zanotelli, M. R., Somasegar, S., Califano, J. P., Montague, C., LaValley, D. J., Huynh, J. et al. (2017). Matrix stiffening promotes a tumor vasculature phenotype. *Proc. Natl. Acad. Sci. USA* **114**, 492-497. doi:10.1073/pnas.1613855114

Bray, S. J. (2016). Notch signalling in context. *Nat. Rev. Mol. Cell Biol.* **17**, 722-735. doi:10.1038/nrm.2016.94

Cui, Y., Zhang, X., You, K., Guo, Y., Liu, C., Fang, X. and Geng, L. (2017). Nanomechanical characteristics of cervical cancer and cervical intraepithelial neoplasia revealed by atomic force microscopy. *Med. Sci. Monit.* **23**, 4205-4213. doi:10.12659/MSM.903484

Das, A., Fischer, R. S., Pan, D. and Waterman, C. M. (2016). YAP nuclear localization in the absence of cell-cell contact is mediated by a filamentous actin-dependent, Myosin II- and Phospho-YAP-independent pathway during extracellular matrix mechanosensing. *J. Biol. Chem.* **291**, 6096-6110. doi:10.1074/jbc.M115.708313

Du, J., Chen, X., Liang, X., Zhang, G., Xu, J., He, L., Zhan, Q., Feng, X. Q., Chien, S. and Yang, C. (2011). Integrin activation and internalization on soft ECM

as a mechanism of induction of stem cell differentiation by ECM elasticity. *Proc. Natl. Acad. Sci. USA* **108**, 9466-9471. doi:10.1073/pnas.1106467108

Estrach, S., Cailleteau, L., Franco, C. A., Gerhardt, H., Stefani, C., Lemichez, E., Gagnoux-Palacios, L., Meneguzzi, G. and Mettouchi, A. (2011). Laminin-binding integrins induce Dll4 expression and Notch signaling in endothelial cells. *Circ. Res.* **109**, 172-182. doi:10.1161/CIRCRESAHA.111.240622

Fernandez-Chacon, M., Garcia-Gonzalez, I., Muhleder, S. and Benedito, R. (2021). Role of Notch in endothelial biology. *Angiogenesis* **24**, 237-250. doi:10.1007/s10456-021-09793-7

Fischer, R. S., Gardel, M., Ma, X., Adelstein, R. S. and Waterman, C. M. (2009). Local cortical tension by myosin II guides 3D endothelial cell branching. *Curr. Biol.* **19**, 260-265. doi:10.1016/j.cub.2008.12.045

Fleige, S., Walf, V., Huch, S., Prgomet, C., Sehm, J. and Pfaffl, M. W. (2006). Comparison of relative mRNA quantification models and the impact of RNA integrity in quantitative real-time RT-PCR. *Biotechnol. Lett.* **28**, 1601-1613. doi:10.1007/s10529-006-9127-2

Gegenfurtner, F. A., Jahn, B., Wagner, H., Ziegenhain, C., Enard, W., Geistlinger, L., Radler, J. O., Vollmar, A. M. and Zahler, S. (2018). Micropatterning as a tool to identify regulatory triggers and kinetics of actin-mediated endothelial mechanosensing. *J. Cell Sci.* **131**, jcs212886. doi:10.1242/jcs.212886

Hodkinson, P. S., Elliott, P. A., Lad, Y., McHugh, B. J., MacKinnon, A. C., Haslett, C. and Sethi, T. (2007). Mammalian NOTCH-1 activates beta1 integrins via the small GTPase R-Ras. *J. Biol. Chem.* **282**, 28991-29001. doi:10.1074/jbc.M703601200

Howe, G. A. and Addison, C. L. (2012). beta1 integrin: an emerging player in the modulation of tumorigenesis and response to therapy. *Cell Adh Migr* **6**, 71-77. doi:10.4161/cam.20077

Koon, Y. L., Zhang, S., Rahmat, M. B., Koh, C. G. and Chiam, K. H. (2018). Enhanced delta-notch lateral inhibition model incorporating intracellular notch heterogeneity and tension-dependent rate of delta-notch binding that reproduces sprouting angiogenesis patterns. *Sci. Rep.* **8**, 9519. doi:10.1038/s41598-018-27645-1

Kwak, M., Southard, K. M., Kim, W. R., Lin, A., Kim, N. H., Gopalappa, R., Lee, H. J., An, M., Choi, S. H., Jung, Y. et al. (2022). Adherens junctions organize size-selective proteolytic hotspots critical for Notch signalling. *Nat. Cell Biol.* **24**, 1739-1753. doi:10.1038/s41556-022-01031-6

Lei, L., Liu, D., Huang, Y., Jovin, I., Shai, S. Y., Kyriakides, T., Ross, R. S. and Giordano, F. J. (2008). Endothelial expression of beta1 integrin is required for embryonic vascular patterning and postnatal vascular remodeling. *Mol. Cell. Biol.* **28**, 794-802. doi:10.1128/MCB.00443-07

Liu, Z. J., Shirakawa, T., Li, Y., Soma, A., Oka, M., Dotto, G. P., Fairman, R. M., Velazquez, O. C. and Herlyn, M. (2003). Regulation of Notch1 and Dll4 by vascular endothelial growth factor in arterial endothelial cells: implications for modulating arteriogenesis and angiogenesis. *Mol. Cell. Biol.* **23**, 14-25. doi:10.1128/MCB.23.1.14-25.2003

Mammoto, A., Connor, K. M., Mammoto, T., Yung, C. W., Huh, D., Aderman, C. M., Mostoslavsky, G., Smith, L. E. and Ingber, D. E. (2009). A mechanosensitive transcriptional mechanism that controls angiogenesis. *Nature* **457**, 1103-1108. doi:10.1038/nature07765

Matsuo, E., Okamoto, T., Ito, A., Kawamoto, E., Asanuma, K., Wada, K., Shimaoka, M., Takao, M. and Shimamoto, A. (2021). Substrate stiffness modulates endothelial cell function via the YAP-Dll4-Notch1 pathway. *Exp. Cell Res.* **408**, 112835. doi:10.1016/j.yexcr.2021.112835

Meloty-Kapella, L., Shergill, B., Kuon, J., Botvinick, E. and Weinmaster, G. (2012). Notch ligand endocytosis generates mechanical pulling force dependent on dynamin, epsins, and actin. *Dev. Cell* **22**, 1299-1312. doi:10.1016/j.devcel.2012.04.005

Merk, H., Zhang, S., Lehr, T., Muller, C., Ulrich, M., Bibb, J. A., Adams, R. H., Bracher, F., Zahler, S., Vollmar, A. M. et al. (2016). Inhibition of endothelial Cdk5 reduces tumor growth by promoting non-productive angiogenesis. *Oncotarget* **7**, 6088-6104. doi:10.18632/oncotarget.6842

Minoguchi, S., Taniguchi, Y., Kato, H., Okazaki, T., Strobl, L. J., Zimber-Strobl, U., Bornkamm, G. W. and Honjo, T. (1997). RBP-L, a transcription factor related to RBP-Jkappa. *Mol. Cell. Biol.* **17**, 2679-2687. doi:10.1128/MCB.17.5.2679

Nandagopal, N., Santat, L. A., LeBon, L., Sprinzak, D., Bronner, M. E. and Elowitz, M. B. (2018). Dynamic ligand discrimination in the notch signaling pathway. *Cell* **172**, 869-880.e19. doi:10.1016/j.cell.2018.01.002

Nichols, J. T., Miyamoto, A., Olsen, S. L., D'Souza, B., Yao, C. and Weinmaster, G. (2007). DSL ligand endocytosis physically dissociates Notch1 heterodimers before activating proteolysis can occur. *J. Cell Biol.* **176**, 445-458. doi:10.1083/jcb.200609014

Nukuda, A., Sasaki, C., Ishihara, S., Mizutani, T., Nakamura, K., Ayabe, T., Kawabata, K. and Haga, H. (2015). Stiff substrates increase YAP-signaling-mediated matrix metalloproteinase-7 expression. *Oncogenesis* **4**, e165. doi:10.1038/oncsis.2015.24

Pauty, J., Usuba, R., Cheng, I. G., Hespel, L., Takahashi, H., Kato, K., Kobayashi, M., Nakajima, H., Lee, E., Yger, F. et al. (2018). A vascular endothelial growth factor-dependent sprouting angiogenesis assay based on an in vitro human blood vessel model for the study of anti-angiogenic drugs. *EBioMedicine* **27**, 225-236. doi:10.1016/j.ebiom.2017.12.014

Perfahl, H., Hughes, B. D., Alarcon, T., Maini, P. K., Lloyd, M. C., Reuss, M. and Byrne, H. M. (2017). 3D hybrid modelling of vascular network formation. *J. Theor. Biol.* **414**, 254-268. doi:10.1016/j.jtbi.2016.11.013

Rallis, C., Pinchin, S. M. and Ish-Horowicz, D. (2010). Cell-autonomous integrin control of Wnt and Notch signalling during somitogenesis. *Development* **137**, 3591-3601. doi:10.1242/dev.050070

Rand, M. D., Grimm, L. M., Artavanis-Tsakonas, S., Patriub, V., Blacklow, S. C., Sklar, J. and Aster, J. C. (2000). Calcium depletion dissociates and activates heterodimeric notch receptors. *Mol. Cell. Biol.* **20**, 1825-1835. doi:10.1128/MCB.20.5.1825-1835.2000

Santos-Oliveira, P., Correia, A., Rodrigues, T., Ribeiro-Rodrigues, T. M., Matafome, P., Rodriguez-Manzaneque, J. C., Seica, R., Girao, H. and Travasso, R. D. (2015). The force at the tip–modelling tension and proliferation in sprouting angiogenesis. *PLoS Comput. Biol.* **11**, e1004436. doi:10.1371/journal.pcbi.1004436

Shamloo, A., Mohammadaliha, N., Heilshorn, S. C. and Bauer, A. L. (2016). A comparative study of collagen matrix density effect on endothelial sprout formation using experimental and computational approaches. *Ann. Biomed. Eng.* **44**, 929-941. doi:10.1007/s10439-015-1416-2

Shaya, O., Binshtok, U., Hersch, M., Rivkin, D., Weinreb, S., Amir-Zilberstein, L., Khamaisi, B., Oppenheim, O., Desai, R. A., Goodyear, R. J. et al. (2017). Cell-cell contact area affects notch signaling and notch-dependent patterning. *Dev. Cell* **40**, 505-511.e6. doi:10.1016/j.devcel.2017.02.009

Shergill, B., Meloty-Kapella, L., Musse, A. A., Weinmaster, G. and Botvinick, E. (2012). Optical tweezers studies on Notch: single-molecule interaction strength is independent of ligand endocytosis. *Dev. Cell* **22**, 1313-1320. doi:10.1016/j.devcel.2012.04.007

Sprinzak, D. and Blacklow, S. C. (2021). Biophysics of notch signaling. *Annu. Rev. Biophys.* **50**, 157-189. doi:10.1146/annurev-biophys-101920-082204

Sprinzak, D., Lakhanpal, A., Lebon, L., Santat, L. A., Fontes, M. E., Anderson, G. A., Garcia-Ojalvo, J. and Elowitz, M. B. (2010). Cis-interactions between Notch and Delta generate mutually exclusive signalling states. *Nature* **465**, 86-90. doi:10.1038/nature08959

Stepanova, D., Byrne, H. M., Maini, P. K. and Alarcon, T. (2021). A multiscale model of complex endothelial cell dynamics in early angiogenesis. *PLoS Comput. Biol.* **17**, e1008055. doi:10.1371/journal.pcbi.1008055

Takeshita, K., Satoh, M., Ii, M., Silver, M., Limbourg, F. P., Mukai, Y., Rikitake, Y., Radtke, F., Gridley, T., Losordo, D. W. et al. (2007). Critical role of endothelial Notch1 signaling in postnatal angiogenesis. *Circ. Res.* **100**, 70-78. doi:10.1161/01.RES.0000254788.47304.6e

Totaro, A., Castellan, M., Di Biagio, D. and Piccolo, S. (2018). Crosstalk between YAP/TAZ and Notch Signaling. *Trends Cell Biol.* **28**, 560-573. doi:10.1016/j.tcb.2018.03.001

Tremblay, I., Pare, E., Arsenault, D., Douziech, M. and Boucher, M. J. (2013). The MEK/ERK pathway promotes NOTCH signalling in pancreatic cancer cells. *PLoS One* **8**, e85502. doi:10.1371/journal.pone.0085502

Yasuda, D., Kobayashi, D., Akahoshi, N., Ohto-Nakanishi, T., Yoshioka, K., Takuwa, Y., Mizuno, S., Takahashi, S. and Ishii, S. (2019). Lysophosphatidic acid-induced YAP/TAZ activation promotes developmental angiogenesis by repressing Notch ligand Dll4. *J. Clin. Invest.* **129**, 4332-4349. doi:10.1172/JCI121955

Zanotelli, M. R. and Reinhart-King, C. A. (2018). Mechanical forces in tumor angiogenesis. *Adv. Exp. Med. Biol.* **1092**, 91-112. doi:10.1007/978-3-319-95294-9_6

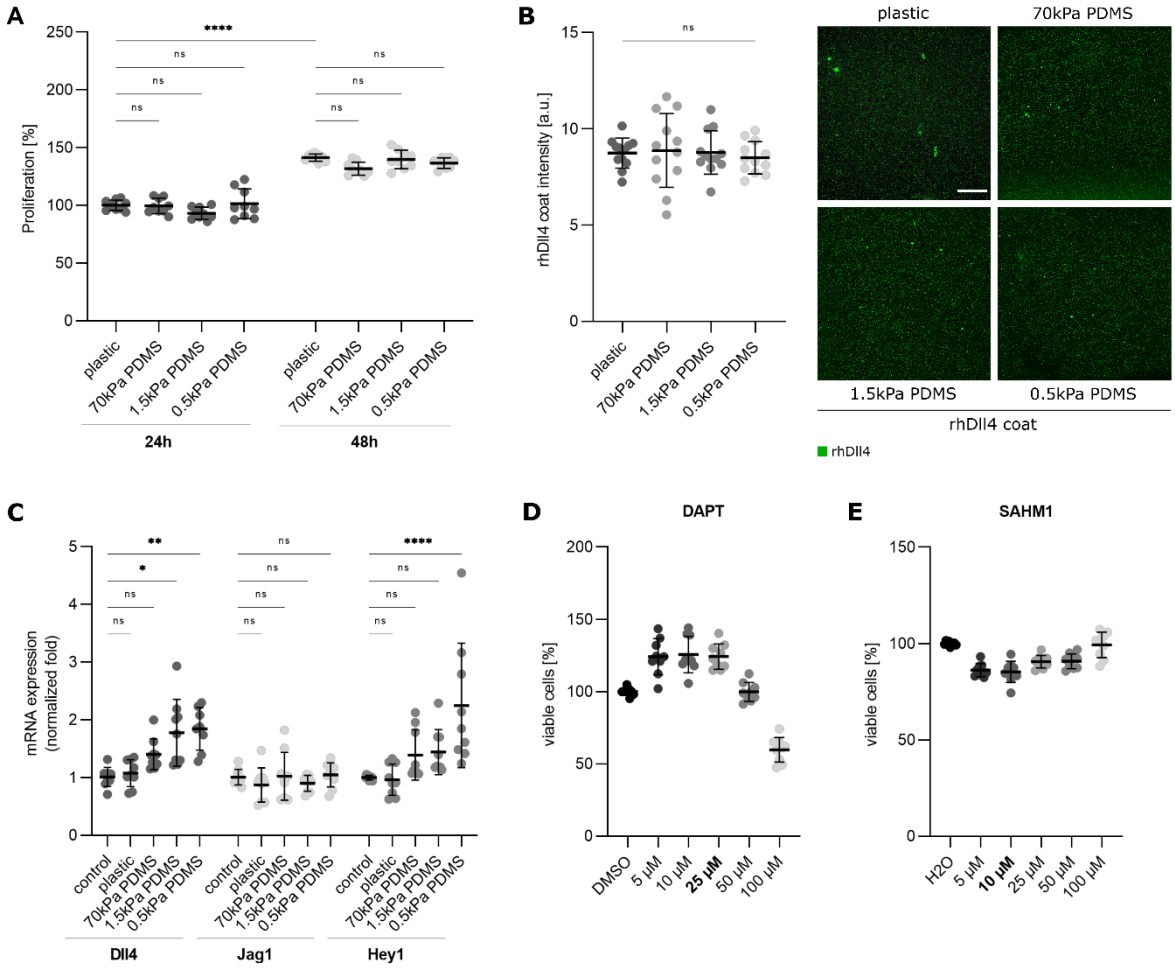

Fig. S1. General proliferation and protein coating on the PDMS substrates are not stiffness dependent and the applied inhibitor concentrations do not have a cytotoxic effect on the cells.

(A) Proliferation of HUVEC cells on substrates with different stiffnesses, incubated for 24h and 48h. Data from three independent experiments, each with triplicates, are shown in scatter plots as mean values ± SD (two-way ANOVA followed by Tukey's multiple comparison test, ns ≙ not significant, ****P<0.0001). (B) PDMS substrates were coated with rhDll4 and stained for Dll4 (shown in green). rhDll4 binding efficiency was compared by evaluation of intensity and the number of particles, summarized in a scatter plot on the left panel (three independent experiments, mean ± SD, one-way ANOVA followed by Tukey's multiple comparison test, ns ≙ not significant). (C) Normalized fold mRNA expression of the Notch ligands Dll4, Jag1 and the Notch target gene Hey1 in HUVECs, outlined in a scatter plot (three independent experiments, each with triplicates, mean ± SD, one-way ANOVA followed by Tukey's multiple comparison test, ns ≙ not significant, *P<0.1, **P<0.01, ****P<0.0001). Induction of Notch activity by coating with rhDll4. Data was normalized to cells on plastic without Notch activation. (D, E) CellTiter-Blue viability assay in HUVEC cells. Cells were treated with the Notch inhibitors DAPT (D) or SAHM1 (E) at different concentrations for 24h. Cell viability is shown in a scatter plot as mean values ± SD (three independent experiments, each with triplicates). The concentrations used for Notch inhibition are indicated in bold.

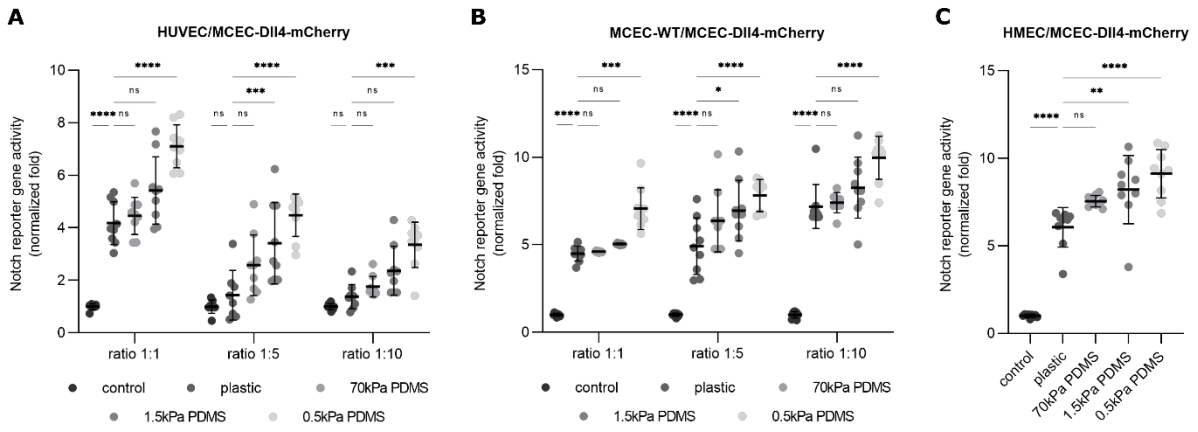

Fig. S2. Notch activation by co-culture of Notch sender and receiver cells increases in soft substrates in all Notch receiver cells but is dependent on the seeding ratio.

(A, B) Normalized fold Notch activity in endothelial co-cultures of HUVEC/MCEC-Dll4-mCherry cells (A) and MCEC-WT/MCEC-Dll4-mCherry cells (B) in seeding ratios of 1:1, 1:5 and 1:10. Scatter plots were generated by evaluation of reporter gene assays on substrates with different stiffnesses (three independent experiments, each with triplicates, two-way ANOVA followed by Tukey's multiple comparison test, ns ≙ not significant, *P<0.1, ****P<0.0001). Data was normalized to cells on plastic without Notch activation (in co-culture with untransfected HUVEC/MCEC-WT cells). (C) Normalized fold Notch activity in HMEC/MCEC-Dll4-mCherry co-culture ratio 1:1, outlined in a scatter plot (three independent experiments, each with triplicates, mean ± SD, one-way ANOVA followed by Tukey's multiple comparison test, ns ≙ not significant, **P<0.01, ****P<0.0001). Data was normalized to cells on plastic without Notch activation (in co-culture with untransfected HMEC cells).

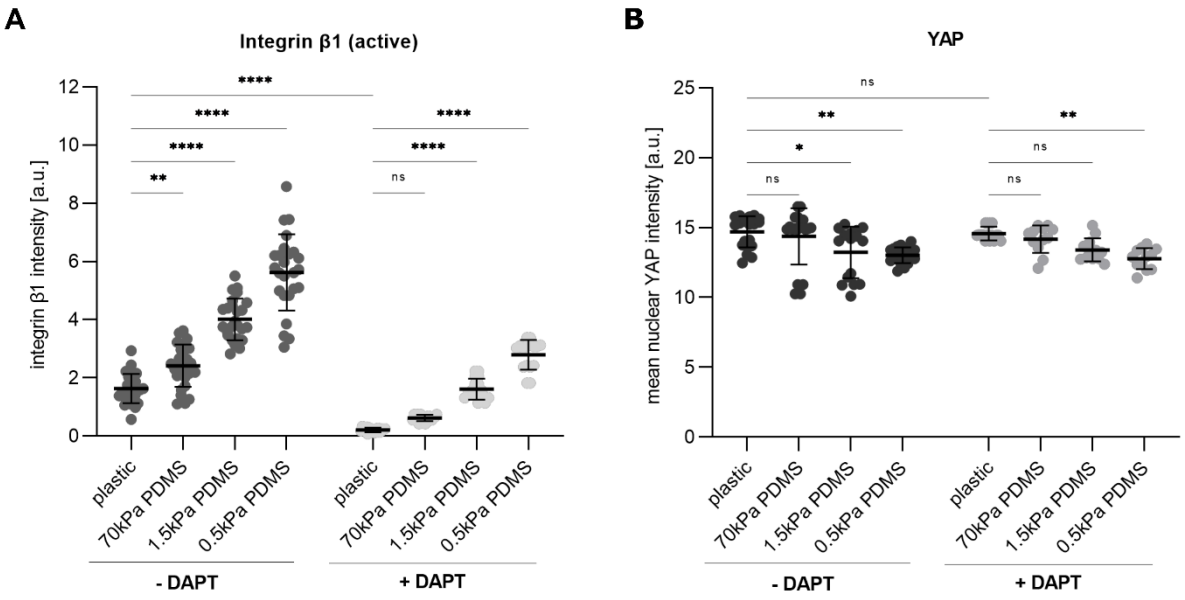

Fig. S3. Integrin β1 intensity in MCEC-WT cells is dependent on substrate stiffness as well as the Notch signaling pathway, whereas the nuclear intensity of YAP does not change after Notch inhibition by DAPT.

(A, B) MCEC-WT cells were seeded on varying substrate stiffness, treated with 25μM DAPT for 24h and stained for either the activated form of integrin β1 or YAP. The mean overall intensity for integrin β1 and the nuclear intensities for YAP ± SD of ≤ 240 untreated and treated cells derived from three independent experiments are summarized in scatter graphs (two-way ANOVA followed by Tukey's multiple comparison test, ns ≙ not significant, **P<0.01, ****P<0.0001). Integrin intensities were analyzed in segmented images. YAP intensities were analyzed with the Intensity Ratio Nuclei Cytoplasm Tool plugin for ImageJ.

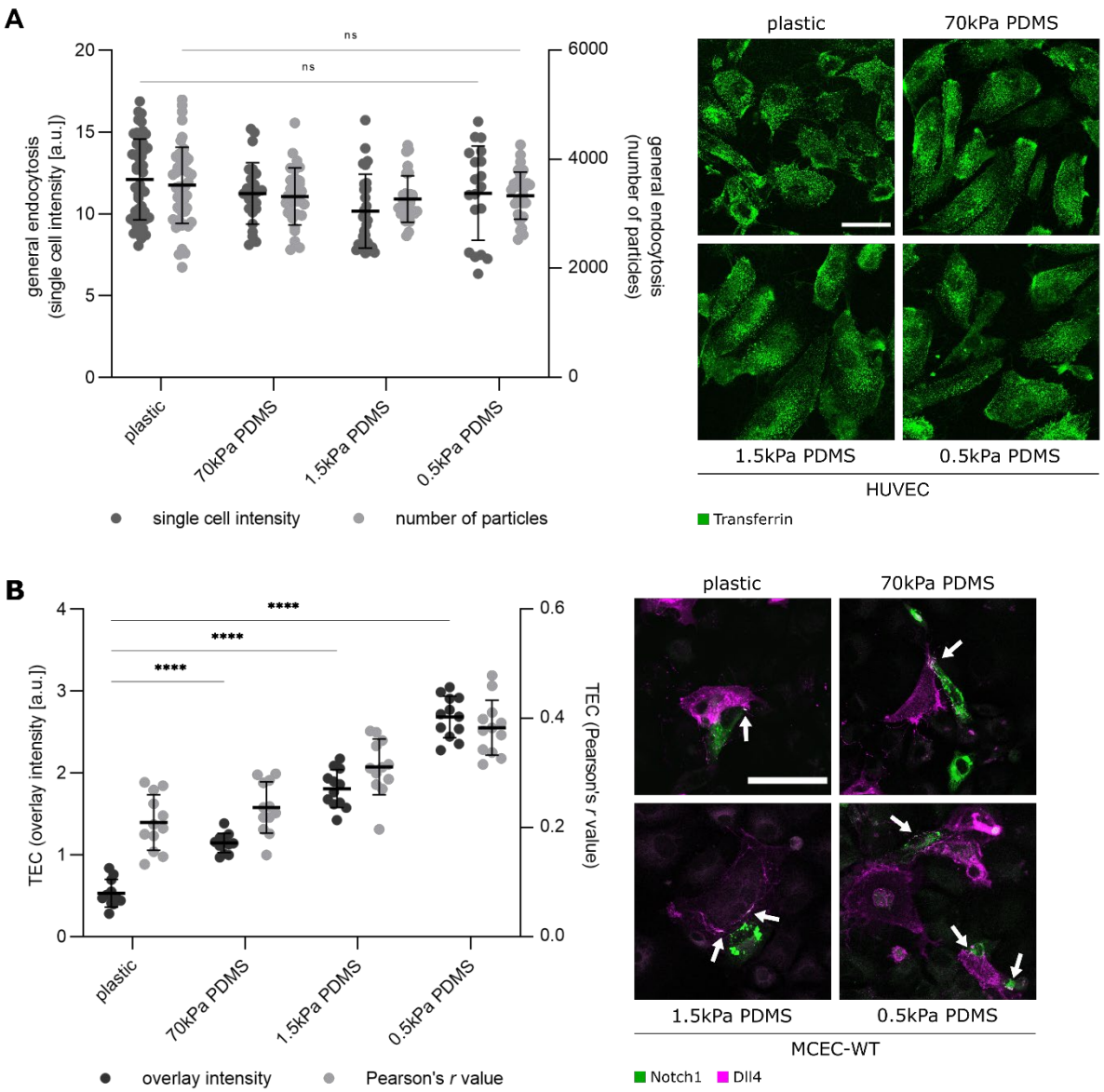

Fig. S4. General endocytosis is not affected by stiffness and trans-endocytosis in MCEC-WT cells is also increased on softer substrates.

(A) General endocytosis in HUCEC. Cells were seeded on substrates with different stiffness and a transferrin endocytosis assay was conducted. Intensity and number of particles in individual cells are presented in a scatter plot as means ± SD of ≥ 240 cells per substrate condition, derived from three independent experiments (two-way ANOVA followed by Tukey's multiple comparison test, ns ≙ not significant) Both intensity and particle number were determined in segmented images and ROIs of the cells. (B) Overlay intensity and Pearson's r value in areas of Notch receptor ligand interactions in the course of trans-endocytosis. Overlay areas are indicated by the white arrows. MCEC-WT cells were transfected separately with a citrine-coupled Notch1 plasmid and a mCherry-coupled Dll4 plasmid. Notch1 expressing Notch receiver cells are shown in green, Dll4 expressing Notch sender cells are shown in magenta. Trans-endocytosis was quantified at cell-cell contacts in ≥ 12 cells per substrate condition in three independent experiments. Data is presented as a scatter plot (mean value ± SD, two-way ANOVA with Tukey's multiple comparison test, ****P<0.0001).